Operator splitting based structure-preserving numerical schemes for the mass-conserving convective Allen-Cahn equation

Rihui Lan^a, Jingwei Li^b, Yongyong Cai^b, Lili Ju^{a,*}

^aDepartment of Mathematics, University of South Carolina, Columbia, SC 29208, USA
^bLaboratory of Mathematics and Complex Systems and School of Mathematical Sciences, Beijing Normal University,
Beijing 100875, China

Abstract

The mass-conserving convective Allen-Cahn (MCAC) equation is an important component of phase field modeling for the multiphase fluid coupled with a flow field. It inherits the maximum bound principle (MBP) from the classic Allen-Cahn equation, in the sense that the time-dependent solution under appropriate initial and boundary conditions preserves a uniform point-wise bound in the absolute value for all time. In this paper, we develop two structure-preserving numerical schemes for the MCAC equation based on the operator splitting approach. In particular, the advancing of the MCAC equation at each time step is split into two (first-order splitting in time) or three (second-order splitting in time) stages, and each of the stages consists of either a mass-conserving AC equation or a transport equation. The mass-conserving AC part is then discretized by using the classic finite volume approximation in space and the stabilized exponential time differencings in time and the resulting system can be efficiently solved via fast Fourier transform based algorithms. The transport part is solved by explicit strong stability preserving Runge-Kutta substeppings combined with a maximum-principle-satisfying finite volume method. Optimal error estimates are derived for the proposed fully-discrete schemes, as well as preservation of the discrete MBP and conservation of the mass. Various numerical examples are also presented to verify the theoretical results and demonstrate the performance of the proposed schemes.

Keywords: Convective Allen–Cahn equation, mass conservation, maximum bound principle, operator splitting method, exponential time differencing, reconstruction

1. Introduction

The flows with multiple constitutive components have occurred in many important industrial problems, such as the drop coalescence and retraction in viscoelastic fluids [57]. The phase field method (or the diffuse interface method) [2, 17, 56, 46] is a very popular approach for modeling the motion of multiphase flows, for instance, the Cahn-Hilliard (CH) equation and the Allen-Cahn (AC) equation, which have been commonly used as two classic phase field models in the past decades

^{*}Corresponding author

Email addresses: rlan@mailbox.sc.edu (Rihui Lan), jingwei@bnu.edu.cn (Jingwei Li), yongyong.cai@bnu.edu.cn (Yongyong Cai), ju@math.sc.edu (Lili Ju)

(see [4, 1, 8, 6, 40, 11] and the references cited therein). Introducing the free energy functional

$$E[u] = \frac{\epsilon^2}{2} (\nabla u, \nabla u) + (F(u), 1), \tag{1}$$

where ∇ is the gradient operator, (\cdot, \cdot) is the standard L^2 inner product and F(u) gives a potential function, the CH equation is a fourth-order (in space) equation and viewed as the H^{-1} -gradient flow of E[u], while the AC equation is a second-order equation and regarded as the L^2 -gradient flow of E[u]. Our study in this work focuses on the AC equation. It is well-known that the CH equation conserves the total mass but the classic AC equation does not. The mass conservation is often an indispensable structure for many physical phenomena and so does the phase-filed model coupled with incompressible flows.

In [56], a mass-conserving fluid-transported AC equation was derived using an energetic variational approach in the following general form:

$$\begin{cases} \frac{\partial u}{\partial t} + \mathbf{v} \cdot \nabla u = \epsilon^2 \Delta u + f(u) - \lambda(t), & \mathbf{x} \in \Omega, t > 0, \\ \frac{d}{dt} \int_{\Omega} u \, d\mathbf{x} = 0, \end{cases}$$
 (2)

where $\Omega \in \mathbb{R}^d$ (d=2,3) is an open, bounded Lipschitz domain, $\Delta = \nabla^2$ is the Laplacian operator, the unknown $u(\boldsymbol{x},t) \in \mathbb{R}$ is the order parameter, $\mathbf{v}(\boldsymbol{x},t) \in \mathbb{R}^d$ is the bulk incompressible velocity field (i.e., $\nabla \cdot \mathbf{v} = 0$), f = -F' is a nonlinear function, and ϵ is a parameter related to the thickness of the transition layers. Here, $\lambda(t)$ plays a role of the Lagrangian multiplier to conserve the mass along the time. When the velocity field \mathbf{v} is not present, J. Rubinstein and P. Sternberg [44] proposed to set

$$\lambda(t) = \frac{1}{|\Omega|} \int_{\Omega} f(u(\boldsymbol{x}, t)) d\boldsymbol{x}$$
(3)

 $(|\Omega|)$ is the Lebesgue measure of Ω) to establish the so-called mass-conserving AC (MAC) equation:

$$\frac{\partial u}{\partial t} = \epsilon^2 \Delta u + \bar{f}(u) \tag{4}$$

with $\bar{f}(u) = f(u) - \frac{1}{|\Omega|} \int_{\Omega} f(u) dx$. Therefore, we consider in this paper the following mass-conserving convective Allen-Cahn (MCAC) equation:

$$\frac{\partial u}{\partial t} + \mathbf{v} \cdot \nabla u = \epsilon^2 \Delta u + \bar{f}(u). \tag{5}$$

Under suitable boundary conditions, it is easy to verify that the classic Allen-Cahn equation [1] satisfies the dissipation law with respect to the energy (1) in the sense that

$$\frac{d}{dt}E[u] = \int_{\Omega} \frac{\delta E}{\delta u} \frac{\partial u}{\partial t} d\mathbf{x} = -\int_{\Omega} \left| \epsilon^2 \Delta u + f(u) \right|^2 d\mathbf{x} \le 0.$$
 (6)

The MAC equation (4) inherits this same energy decaying property (6) as it was derived by minimizing E[u] under the mass-conservation constraint. However, such energy dissipation can not be theoretically guaranteed anymore for the MCAC equation (5).

The maximum bound principle (MBP) is another important structure of the AC equation [1]. We will show that MCAC equation also shares this property in the sense that if the initial value and/or the boundary values are point-wisely bounded by a specific constant in the absolute value, then the solution is also bounded by the same constant everywhere for all time. MBP is an useful mathematical tool to study physical features of the AC-type equation [15, 43], especially for the logarithmic type potential $F(\cdot)$. In this case, if the numerical scheme does not satisfy the MBP. complex values may occur in the numerical simulations due to the logarithm arithmetic, which could further lead to unphysical solutions. For the classic AC equation, discrete MBP-preserving numerical methods have been thoroughly studied in recent years. For its spatial discretization, a partial list includes the works on the lumped-mass finite element method [53], finite difference method [25], finite volume method [42] and so on. For its temporal integration, the stabilized linear semi-implicit schemes [51, 54] were shown to preserve the MBP unconditionally for the firstorder scheme and conditionally for the second-order scheme. In [34], H. Liao et al. show the second order BDF scheme with variable time steps is energy stable, and conditionally preserves the MBP. Some nonlinear second-order schemes were presented in [35] which preserve the MBP for the time-fractional AC-type equations. In addition, some cut-off postprocessing methods were studied in [28, 55] to preserve the MBP. For the MAC equation, energy-dissipative and mass-conserving schemes were designed in [27] by introducing two different mass correction operators. In [45], Shen et al. investigated the stabilizing MBP-preserving schemes for the convective Allen-Cahn equation using the finite difference discretization with the upwind scheme in space, and later Shen and Zhang designed a MBP-preserving scheme with a higher-order accurate finite difference scheme in [47]. However, both of them only considered the first-order implicit explicit (IMEX) scheme in time.

The exponential time differencing (ETD) method [3, 10, 20] was recently applied with the stabilizing technique to preserve the MBP for semilinear parabolic equation in [12, 13]. Based on the Duhamel's formula, the ETD methods integrate the temporal integrals exactly after approximating the nonlinear terms by polynomial interpolations. The ETD method is applicable to a large class of equations, particularly those with a stiff linear part [32, 25, 26, 7, 9]. The first- and secondorder stabilized ETD schemes were first applied to the nonlocal Allen-Cahn equation [12] with unconditional preservation of the MBP, and then in [13] an abstract framework for MBP-preserving ETDRK schemes was established, which was later further extended to the conservative Allen-Cahn equations in [29, 23]. Recently, some third- and fourth-order MBP-preserving schemes for the Allen-Cahn equation were developed in [22, 30, 24, 60] based on the integrating factor Runge-Kutta (IFRK) method, and an arbitrarily high-order ETD multistep method was proposed by enforcing the maximum bound with extra cut-off postprocessing in [28]. The major computational cost of the ETD method comes from the action of the matrix exponential on a vector, and the Krylov subspace method [41, 16] provides an effective way for its calculation. If the spatial mesh is regular, fast Fourier transform (FFT) based algorithms could be employed to further improve the efficiency [26]. As an important component of the model equation (5), the convective term may increase the difficulty of constructing efficient MBP-preserving numerical schemes. There exist several works on preserving the MBP for the convective Allen-Cahn equation by utilizing the upwind strategy for spatial discretization. In [45], a first-order unconditionally MBP-preserving numerical scheme was designed by using the upwind finite difference method. Later first- and second-order unconditionally MBP-preserving upwind ETD schemes were proposed in [5]. However, the resulting linear systems in those upwind methods involve variable-coefficients due to the convective term and consequently causes the failure of the FFT-based fast solvers. Moreover, the upwind strategy leads to the firstorder accuracy in space with certain strict CFL stability conditions [59], thus is hard to capture well the dynamical interface behavior of phase evolution in practice.

To improve the spatial accuracy, we must take good care of the convective term in (5) and design higher order spatial approximations for the flux. Essentially, we plan to treat the convective term as a transport equation corresponding to the conservation law since there have been many efficient high-order numerical schemes for its treatment. Among them the essentially non-oscillatory (ENO) and weighted essentially non-oscillatory (WENO) schemes [49, 39, 48] have been widely studied. Liu and Osher [38] designed the third-order scheme in the sense of flux approximation which preserves the local maximum principle and the non-oscillatory property by introducing the limiter. However, such limiter depends on the maximum value of the reconstruction polynomial over the chosen stencils, and is difficult to implement in high dimensional spaces. Later on, Liu and Osher's limiter was relaxed in [61] by focusing on finding the maximum value of the reconstruction polynomial on the quadrature points instead of the whole cell, and maximum-principle-satisfying high-order schemes were successfully developed under the finite volume and discontinuous Galerkin frameworks.

Our paper aims to design structure-preserving (i.e., MBP-preserving and mass-conserving) efficient numerical methods for the MCAC equation (5). Motivated by [33, 58, 36, 37], we first use the operator splitting method to decouple the MCAC equation at each time step into a split system consisting of MAC and transport equations. The resulting MAC equations naturally satisfy the MBP and can be efficiently solved by the stabilized ETD schemes with FFT as discussed above. At the same time, the limiter-based maximum-principle-satisfying finite volume scheme [61] with explicit strong stability preserving Runge-Kutta (SSPRK) stepping is adopted to solve the resulting transport equation.

The rest of this paper is organized as follows. In Section 2 we briefly review and derive the conditions for the MCAC equation to satisfy the MBP. In Section 3, the first- and second-order operator splitting schemes are first presented which decouple the MCAC equation into some transport and MAC equations, then the corresponding subsystem solvers are discussed in detail. In Section 4, fully discrete schemes for the MCAC equation with MBP-preservation and mass-conservation are proposed together with their error analysis. In Section 5, various numerical experiments are carried out to verify the theoretical results and demonstrate the performance of the proposed schemes. Finally, some concluding remarks are drawn in Section 6.

2. Maximum bound principle for the MCAC equation

Let us briefly review and derive the conditions for the MCAC equation (5) to hold the MBP property. Assume that $f: \text{Dom}(f)(\subset \mathbb{R}) \to \mathbb{R}$ is a continuously differentiable nonlinear function and the initial condition is given by

$$u(\boldsymbol{x},0) = u_0(\boldsymbol{x}), \quad \boldsymbol{x} \in \overline{\Omega}.$$
 (7)

For simplicity, we also assume that the periodic boundary condition is imposed for a rectangular domain $\Omega = \prod_{i=1}^{d} (a_i, b_i)$, and note that the results obtained below also can be easily extended to the homogeneous Neumann boundary condition case. For some appropriate nonlinear function f and velocity field \mathbf{v} , the MCAC equation (5) admits a unique smooth solution by the classic theory for the semilinear parabolic equations [52]. Following the analysis in [44], the following assumption on f is important for establishing the MBP for (5).

Assumption 2.1. There exists a constant $\beta > 0$ such that $[-\beta, \beta] \subset Dom(f)$, $f(\beta) < f(-\beta)$ and

$$f(\beta) \le f(w) \le f(-\beta), \quad \forall w \in [-\beta, \beta].$$

Moreover, for any $\varepsilon > 0$ sufficiently small, it holds that

$$f^{-1}(f(\beta)) \cap (\beta - \varepsilon, \beta) = \emptyset$$
 and $f^{-1}(f(-\beta)) \cap (-\beta, -\beta + \varepsilon) = \emptyset$.

Note that if the function f satisfies $f(M) \leq f(w) \leq f(m)$ for $w \in [m, M]$, then an affine mapping can transform f into the form in Assumption 2.1 as suggested in [29, 13]. Therefore, we only focus on the situation stated in Assumption 2.1. Two such typical potentials are widely used in phase field modeling: one is the double-well potential:

$$F(u) = \frac{1}{4} (u^2 - 1)^2, \quad f(u) = u - u^3, \tag{8}$$

where $\text{Dom}(f) = \mathbb{R}$ and $\beta \in \left[\frac{2\sqrt{3}}{3}, \infty\right)$, and the other is the Flory-Huggins potential:

$$F(u) = \frac{\theta}{2} \left[(1+u) \ln(1+u) + (1-u) \ln(1-u) \right] - \frac{\theta_c}{2} u^2, \quad f(u) = \frac{\theta}{2} \ln \frac{1-u}{1+u} + \theta_c u, \tag{9}$$

where $\theta_c > \theta > 0$, Dom(f) = (-1,1) and $\beta \in [\rho,1)$ with ρ denoting the positive root of $f(\rho) = f\left(-\sqrt{1-\frac{\theta}{\theta_c}}\right)$.

Given a terminal time T > 0, under Assumption 2.1, we can show that the MCAC equation (5) satisfies the MBP as stated in the following proposition.

Proposition 2.2. [MBP for the MCAC equation] Suppose that the Assumption 2.1 is satisfied, $\mathbf{v} \in C([0,T]; [C^1(\Omega)]^d) \cap C([0,T] \times \overline{\Omega})$, and $u \in C^1((0,T); C^2(\Omega)) \cap C([0,T]; C^1(\overline{\Omega}))$ is a solution to the problem (5) on the time interval [0,T]. If the initial value $||u_0||_{\infty} \leq \beta$ ($||\cdot||_{\infty}$ is the L^{∞} norm), there holds

$$||u(\cdot,t)||_{\infty} \le \beta, \quad \forall t \in [0,T].$$

Proof. Define $t_* = \max \{0 \le t \le T | \|u(\cdot,s)\|_{\infty} \le \beta, \forall s \in [0,t] \}$ and t_* is well-defined by the continuity assumptions on the exact solution $u(\boldsymbol{x},t)$. Thus we need to show $t_* = T$. By contraction, we suppose that $0 \le t_* < T$ such that $\|u(\cdot,t_*)\|_{\infty} = \beta$. Then there exists a sequence $\{t_k\}$ such that $t_k \downarrow t_*$ and $\|u(\cdot,t_k)\|_{\infty} > \beta$ $(k=1,2,\cdots)$. Let us choose $\{\boldsymbol{x}_k\}$ with $|u(\boldsymbol{x}_k,t_k)| = \|u(\cdot,t_k)\|_{\infty} > \beta$, then for some convergent subsequence $\boldsymbol{x}_k \to \boldsymbol{x}_* \in \Omega$ (denoted as the original sequence $\{\boldsymbol{x}_k\}$ for simplicity), we have $u(\boldsymbol{x}_*,t_*) = \beta$ and $u(\boldsymbol{x}_k,t_k) > \beta$ as $t_k \to t_*$, $\boldsymbol{x}_k \to \boldsymbol{x}_*$ (or $u(\boldsymbol{x}_*,t_*) = -\beta$ and $u(\boldsymbol{x}_k,t_k) < -\beta$). Without loss of generality, let us assume $u(\boldsymbol{x}_*,t_*) = \beta$ and $u(\boldsymbol{x}_k,t_k) > \beta$. Due to the periodic boundary condition, we can simply treat $\boldsymbol{x}_* \in \Omega$ (since the gradient $\nabla u(\cdot,t_*)$ vanishes at \boldsymbol{x}_* if \boldsymbol{x}_* is on the boundary), and the following estimates hold by Taylor expansion

$$\frac{\partial u}{\partial t}(\boldsymbol{x}_*, t_*) \ge 0 \text{ and } \epsilon^2 \Delta u(\boldsymbol{x}_*, t_*) \le 0.$$
 (10)

Based on (10) and the equation (5), we then obtain

$$\bar{f}(u(\boldsymbol{x}_*, t_*)) - \nabla \cdot (\mathbf{v}u)|_{(\boldsymbol{x}_*, t_*)} \ge 0.$$

Recalling $\nabla \cdot \mathbf{v} = 0$ and $\nabla u(\mathbf{x}_*, t_*) = 0$, it can be further reduced to

$$\bar{f}(u(\boldsymbol{x}_*, t_*)) = f(\beta) - \frac{1}{|\Omega|} \int_{\Omega} f(u(\boldsymbol{x}, t_*)) d\boldsymbol{x} \ge 0.$$
(11)

On the other hand, since $f(u(\boldsymbol{x},t_*)) \geq f(\beta)$ for any $\boldsymbol{x} \in \overline{\Omega}$, we have

$$f(\beta) - \frac{1}{|\Omega|} \int_{\Omega} f(u(\boldsymbol{x}, t_*)) d\boldsymbol{x} \le 0$$

and the equality holds if and only if $f(u(\boldsymbol{x},t_*)) \equiv f(\beta)$. If $u(\boldsymbol{x},t_*)$ is not a constant function on Ω , the continuity and the Assumption 2.1 would imply $f(\beta) - \frac{1}{|\Omega|} \int_{\Omega} f(u(\boldsymbol{x},t_*)) d\boldsymbol{x} < 0$, contradicting (11). On the other hand, if $u(\boldsymbol{x},t_*) = \beta$ is a constant for all $\boldsymbol{x} \in \Omega$, it follows that $u(\boldsymbol{x},t) = \beta$ is the solution to the equation (5) for all $t > t_*, \boldsymbol{x} \in \Omega$. This contradicts the assumption $t_* < T$. To conclude, we have $t_* = T$ and the proof is completed.

It is worth noting that under the framework in [13, 14], the Laplacian operator Δ generates a contraction semigroup $\{S_{\Delta}(t)\}_{t\geq 0}$ with respect to the supremum norm on the subspace of $C(\overline{\Omega})$ satisfying the periodic boundary condition. Moreover, we have the following lemma regarding the semigroup generated by $A = \Delta - \alpha \mathcal{I}$, where \mathcal{I} is the identity operator and $\alpha \geq 0$ is a constant.

Lemma 2.3. [13] The operator A generates a contraction semigroup $\{S_A(t)\}_{t\geq 0}$ with respect to the supremum norm on the subspace of $C(\overline{\Omega})$ that satisfies the periodic boundary condition. Furthermore, it holds

$$\|\mathcal{S}_{\mathcal{A}}(t)u\|_{\infty} \leq e^{-\alpha t} \|u\|_{\infty}, \quad \forall \, u \in C(\overline{\Omega}), \, t \geq 0.$$

Thanks to Lemma 2.3, we next introduce a constant parameter $\kappa > 0$ for the MCAC equation (5) for the purpose of stabilizing its nonlinear term in the temporal discretization. Note that $\nabla \cdot (\mathbf{v}u) = \mathbf{v} \cdot \nabla u$ since $\nabla \cdot \mathbf{v} = 0$. Let us reformulate (5) in the following equivalent form:

$$\frac{\partial u}{\partial t} + \nabla \cdot (\mathbf{v}u) = \mathcal{L}_{\kappa} u + \bar{f}_{\kappa}(u), \quad \boldsymbol{x} \in \Omega, \ 0 < t \le T, \tag{12}$$

where $\mathcal{L}_{\kappa} = \epsilon^2 \Delta - \kappa \mathcal{I}$, $\bar{f}_{\kappa}(u) = \kappa u + \bar{f}(u)$ and the stabilizing constant κ satisfies

$$\kappa \ge \max_{|\xi| \le \beta} |f'(\xi)|. \tag{13}$$

Note that κ in (13) is always well-defined since f is continuously differentiable. Furthermore, the nonlinear term $\bar{f}_{\kappa}(u)$ bears the following properties.

Lemma 2.4. [29] Under Assumption 2.1 and the requirement (13), it holds that

- (I) $|\bar{f}_{\kappa}(\xi)| \leq \kappa \beta$ for any $\xi \in [-\beta, \beta]$;
- (II) $|\bar{f}_{\kappa}(\xi_1) \bar{f}_{\kappa}(\xi_2)| \le 3\kappa |\xi_1 \xi_2|$ for any $\xi_1, \xi_2 \in [-\beta, \beta]$.

3. Operator splitting method for the MCAC equation and subsystem solvers

In this section, we will consider the operator splitting method and corresponding subsystem solvers for solution of the stabilized equation (12) (which is equivalent to the original MCAC

equation (5)). Choosing a uniform time step size $\tau = \frac{T}{N}$ with N > 0 an integer, we have the time steps as $\{t_n = n\tau\}_{n=0}^N$.

3.1. Operator splitting schemes

The operator splitting technique is adopted to decouple the convection part and the MAC part of (12). According to [21], the first-order operator splitting (in time) of (12) containing two stages can be expressed as: given $u^0(\mathbf{x}) = u_0(\mathbf{x})$, for $n = 0, 1, \dots, N-1$, find $u^{n+1}(\mathbf{x}) = u^{**}(\mathbf{x}, \tau)$ such that

$$\begin{cases}
\frac{\partial u^*(\boldsymbol{x},s)}{\partial s} = \mathcal{L}_{\kappa} u^*(\boldsymbol{x},s) + \bar{f}_{\kappa}(u^*(\boldsymbol{x},s)), \ s \in [0,\tau] \quad \& \ u^*(\boldsymbol{x},0) = u^n(\boldsymbol{x}), \quad (\text{MAC}) \\
\frac{\partial u^{**}(\boldsymbol{x},s)}{\partial s} = -\nabla \cdot (\mathbf{v}(\boldsymbol{x},t_n+s)u^{**}(\boldsymbol{x},s)), \ s \in [0,\tau] \quad \& \ u^{**}(\boldsymbol{x},0) = u^*(\boldsymbol{x},\tau). \quad (\text{Transport})
\end{cases}$$
(14)

As shown in [21, Chapter IV], the above scheme (14) bears a splitting error of $O(\tau)$ and we state the result in Lemma 3.1.

Lemma 3.1. [21] Assume that $\mathbf{v} \in C^1((0,T); [C^1(\Omega)]^d)$ and the exact solution to the MCAC equation (5) $u \in C^2((0,T); C^2(\Omega))$. Let $\{u^n\}_{n=0}^N$ be the numerical solution produced by the first-order splitting scheme (14). Then there exists a constant C > 0 independent of τ , such that

$$||u(\cdot,t_n) - u^n||_{\infty} \le C\tau, \quad 1 \le n \le N. \tag{15}$$

Next we consider the second-order operator splitting (in time) scheme, also called "Strang splitting", which contains three stages. Since the convection term contains the time-dependent velocity field, we will put the transport equation at the middle stage and the MAC equations at the first and third stages. Then the second-order operator splitting of (12) can be expressed as: given $u^0(\mathbf{x}) = u_0(\mathbf{x})$, for $n = 0, 1, \dots, N - 1$, find $u^{n+1}(\mathbf{x}) = u^{***}(\mathbf{x}, \tau/2)$ such that

$$\begin{cases}
\frac{\partial u^*(\boldsymbol{x},s)}{\partial s} = \mathcal{L}_{\kappa}u^*(\boldsymbol{x},s) + \bar{f}_{\kappa}(u^*(\boldsymbol{x},s)), \ s \in [0,\tau/2] & \& \ u^*(\boldsymbol{x},0) = u^n(\boldsymbol{x}), \quad (\text{MAC}) \\
\frac{\partial u^{**}(\boldsymbol{x},s)}{\partial s} = -\nabla \cdot (\mathbf{v}(\boldsymbol{x},t_n+s)u^{**}(\boldsymbol{x},s)), \ s \in [0,\tau] & \& \ u^{**}(\boldsymbol{x},0) = u^*(\boldsymbol{x},\tau/2), \quad (\text{Transport}) \\
\frac{\partial u^{***}(\boldsymbol{x},s)}{\partial s} = \mathcal{L}_{\kappa}u^{***}(\boldsymbol{x},s) + \bar{f}_{\kappa}(u^{***}(\boldsymbol{x},s)), \ s \in [0,\tau/2] & \& \ u^{***}(\boldsymbol{x},0) = u^{**}(\boldsymbol{x},\tau). \quad (\text{MAC}) \\
\end{cases}$$
(16)

As shown in [21, Chapter IV], the above scheme (16) bears a splitting error of $O(\tau^2)$ and we state the result in Lemma 3.2.

Lemma 3.2. [21] Suppose that $\mathbf{v}(\mathbf{x},t) \in C^2((0,T); [C^2(\Omega)]^d)$ and the exact solution to the MCAC equation (5) $u \in C^3((0,T); C^2(\Omega))$. Let $\{u^n\}_{n=0}^N$ be the numerical solution produced by the second-order splitting scheme (16). There exists a constant C > 0 independent of τ , such that

$$||u(\cdot,t_n) - u^n||_{\infty} \le C\tau^2, \quad 1 \le n \le N.$$

$$\tag{17}$$

We then construct numerical methods for solving the two subsystems: the MAC equations and the transport equations resulting from the operator splitting schemes (14) and (16). To simplify the description, we only discuss the two-dimensional (d=2) case and all results can be easily extended to the three-dimensional (d=3) case. Let us introduce the uniform mesh Ω_h of domain

 Ω as set of nodes $\boldsymbol{x}_{i,j} = (x_i,y_j)$ with $x_i = a_1 + ih$, $y_j = a_2 + jh$, $0 \le i \le N_x$ and $0 \le j \le N_y$, where $h = \frac{b_1 - a_1}{N_x} = \frac{b_2 - a_2}{N_y}$. We will use the finite volume methods for spatial discretization. The control volume $K_{i,j}$ associated with the nodes (x_i,y_j) is defined to be $(x_{i-1/2},x_{i+1/2})\times (y_{j-1/2},y_{j+1/2})$ and set $\Omega_h = \{K_{i,j}\}$. Denote $\bar{u}_{i,j}(t)$ as the cell average of $u(\boldsymbol{x},t)$ on the control volume $K_{i,j}$, i.e., $\bar{u}_{i,j}(t) = \frac{1}{h^2} \int_{K_{i,j}} u(\boldsymbol{x},t) \, d\boldsymbol{x}$ for any $K_{i,j} \in \Omega_h$ and $t \ge 0$. To deal with the period boundary condition, we have $\bar{u}_{N_x \pm i,j}(t) = \bar{u}_{\pm i,j}(t)$ and $\bar{u}_{i,N_y \pm j}(t) = \bar{u}_{i,\pm j}(t)$ for $0 \le i < N_x$ and $0 \le j < N_y$. The discrete L^2 norm $\|\cdot\|_h$, and the L^∞ norm $\|\cdot\|_{\infty,h}$ are respectively given by

$$||u||_h := \sqrt{h^2 \sum_{i=0}^{N_x - 1} \sum_{j=0}^{N_y - 1} u_{i,j}^2}, \quad ||u||_{\infty,h} := \max_{0 \le i \le N_x - 1, 0 \le j \le N_y - 1} |u_{i,j}|,$$

and the discrete total mass $\mathcal{M}(\bar{u})$ is computed by

$$\mathcal{M}(\bar{u}) = \frac{h^2}{4} \sum_{i=0}^{N_x - 1} \sum_{j=0}^{N_y - 1} (\bar{u}_{i,j} + \bar{u}_{i+1,j} + \bar{u}_{i,j+1} + \bar{u}_{i+1,j+1}) = h^2 \sum_{i=0}^{N_x - 1} \sum_{j=0}^{N_y - 1} \bar{u}_{i,j},$$

where the last equality comes from the periodic boundary condition.

3.2. Exponential time differencing finite volume method for the MAC equation

Let us consider the MAC equation (4) with $u(0) = u_0$. Integrating the equation over the control volume $K_{i,j}$ and applying the finite volume approximation, we obtain a space-discrete system as:

$$\frac{\partial \bar{U}_{i,j}(t)}{\partial t} = \epsilon^2 \frac{\bar{U}_{i+1,j}(t) + \bar{U}_{i-1,j}(t) + \bar{U}_{i,j+1}(t) + \bar{U}_{i,j-1}(t) - 4\bar{U}_{i,j}(t)}{h^2} + \bar{f}(\bar{U}_{i,j}(t))$$
(18)

with $\bar{U}_{i,j}(0) = (\bar{u}_0)_{i,j} := \frac{1}{h^2} \int_{K_{i,j}} u_0(\boldsymbol{x}) d\boldsymbol{x}$ and $\bar{f}(\bar{U}_{i,j}(t)) = f(\bar{U}_{i,j}(t)) - \mathcal{M}(f(\bar{U}_{i,j}(t)))$. By denoting Δ_h as the discrete operator of Δ , we can express (18) as

$$\frac{\partial \bar{U}_h(t)}{\partial t} = \epsilon^2 \Delta_h \bar{U}_h(t) + \bar{f}(\bar{U}_h(t)),$$

where $\bar{U}_h(t)$ is the discrete function defined on Ω_h with $\bar{U}_h(x_i, y_j, t) = \bar{U}_{i,j}(t)$. Consequently, we can rewrite (18) in the stabilized form as:

$$\frac{\partial U_h(t)}{\partial t} = \mathcal{L}_{\kappa,h} \bar{U}_h(t) + \bar{f}_{\kappa}(\bar{U}_h(t)), \tag{19}$$

where $\mathcal{L}_{\kappa,h} = \epsilon^2 \Delta_h - \kappa I_h$, and I_h is the identity operator on the discrete grid function. If we regard $\bar{U}_h(t)$ as a vector of length $N_x N_y$ with elements arranged first in x-coordinate then in y-coordinate, then the discrete operators $\mathcal{L}_{\kappa,h}$, Δ_h and I_h also can be regarded as square matrices of dimension $N_x N_y \times N_x N_y$. By modifying the arguments in [50], we can prove the following result.

Lemma 3.3. Suppose that Assumption 2.1 holds, the exact solution to the MAC equation (4) $u \in C^1((0,T); C^4(\Omega))$, and $||u_0(\cdot)||_{\infty} \leq \beta$. Let $\bar{U}_h(t)$ be the numerical solution produced by the scheme (18). There exists a constant C > 0 depending only on u, Ω , T, and ϵ , such that

$$||u(\cdot,t) - \bar{U}_h(\cdot,t)||_{\infty,h} \le Ch^2, \quad \forall t \in [0,T].$$
(20)

Proof. By Taylor expansion, we can approximate u(x,t) on $K_{i,j}$ by

$$u(\boldsymbol{x},t) = u(\boldsymbol{x}_{i,j},t) + \nabla u(\boldsymbol{x}_{i,j},t) \cdot (\boldsymbol{x} - \boldsymbol{x}_{i,j}) + \frac{1}{2}(\boldsymbol{x} - \boldsymbol{x}_{i,j})^2 :: (\nabla \nabla u(\boldsymbol{x}_{i,j},t)) + \frac{1}{6}(\boldsymbol{x} - \boldsymbol{x}_{i,j})^3 ::: (\nabla \nabla \nabla u(\boldsymbol{x}_{i,j},t)) + O(|\boldsymbol{x} - \boldsymbol{x}_{i,j}|^4).$$

Integrating over any $K_{i,j} \in \Omega_h$ and dividing h^2 on both sides, we have

$$\bar{u}_{i,j} = u(\boldsymbol{x}_{i,j}, t) + \int_{K_{i,j}} \frac{(\boldsymbol{x} - \boldsymbol{x}_{i,j})}{h^2} \cdot \nabla u(\boldsymbol{x}_{i,j}, t) + \int_{K_{i,j}} \frac{(\boldsymbol{x} - \boldsymbol{x}_{i,j})^2}{2h^2} :: (\nabla \nabla u(\boldsymbol{x}_{i,j}, t)) \, d\boldsymbol{x}
+ \int_{K_{i,j}} \frac{(\boldsymbol{x} - \boldsymbol{x}_{i,j})^3}{6h^2} ::: (\nabla \nabla \nabla u(\boldsymbol{x}_{i,j}, t)) \, d\boldsymbol{x} + O(h^4)
= u(\boldsymbol{x}_{i,j}, t) + \frac{h^2}{24} \Delta u(\boldsymbol{x}_{i,j}, t) + O(h^4),$$
(21)

where the second equality comes from the fact that $\mathbf{x}_{i,j}$ is the center of $K_{i,j}$ thus $\int_{K_{i,j}} \nabla u(\mathbf{x}_{i,j},t) \cdot (\mathbf{x} - \mathbf{x}_{i,j}) d\mathbf{x} = 0$ and $\int_{K_{i,j}} (\mathbf{x} - \mathbf{x}_{i,j})^3 ::: (\nabla \nabla \nabla u(\mathbf{x}_{i,j},t)) d\mathbf{x} = 0$. The five-point central difference scheme for the Laplacian has second-order accuracy in space, i.e.,

$$\Delta u(\boldsymbol{x}_{i,j},t) = \frac{u(\boldsymbol{x}_{i+1,j},t) + u(\boldsymbol{x}_{i-1,j},t) + u(\boldsymbol{x}_{i,j+1},t) + u(\boldsymbol{x}_{i,j-1},t) - 4u(\boldsymbol{x}_{i,j},t)}{h^2} + O(h^2).$$

Plugging (21) into the above equation, it yields

$$\Delta u(\boldsymbol{x}_{i,j},t) = \frac{\bar{u}_{i+1,j}(t) + \bar{u}_{i-1,j}(t) + \bar{u}_{i,j+1}(t) + \bar{u}_{i,j-1}(t) - 4\bar{u}_{i,j}(t)}{h^2}$$

$$- \frac{h^2}{24} \Delta \frac{u(\boldsymbol{x}_{i+1,j},t) + u(\boldsymbol{x}_{i-1,j},t) + u(\boldsymbol{x}_{i,j+1},t) + u(\boldsymbol{x}_{i,j-1},t) - 4u(\boldsymbol{x}_{i,j},t)}{h^2} + O(h^2)$$

$$= \frac{\bar{u}_{i+1,j}(t) + \bar{u}_{i-1,j}(t) + \bar{u}_{i,j+1}(t) + \bar{u}_{i,j-1}(t) - 4\bar{u}_{i,j}(t)}{h^2} - \frac{h^2}{24} \Delta^2 u(\boldsymbol{x}_{i,j},t) + O(h^2).$$

Hence,

$$\epsilon^2 \Delta u(\boldsymbol{x}_{i,j}, t) = \epsilon^2 \frac{\bar{u}_{i+1,j}(t) + \bar{u}_{i-1,j}(t) + \bar{u}_{i,j+1}(t) + \bar{u}_{i,j-1}(t) - 4\bar{u}_{i,j}(t)}{h^2} + O(h^2).$$
 (22)

Next, we turn to the nonlinear term. Since f is continuously differentiable, we obtain

$$\begin{split} \frac{1}{|\Omega|} \int_{\Omega} f(u(\boldsymbol{x},t)) \, d\boldsymbol{x} &= \frac{1}{|\Omega|} \sum_{i=0}^{N_x - 1} \sum_{j=0}^{N_y - 1} \int_{K_{i,j}} f(u(\boldsymbol{x},t)) \, d\boldsymbol{x} \\ &= \frac{1}{|\Omega|} \sum_{i=0}^{N_x - 1} \sum_{j=0}^{N_y - 1} \int_{K_{i,j}} f(\bar{u}_{i,j}(t)) \, d\boldsymbol{x} + \frac{1}{|\Omega|} \sum_{i=0}^{N_x - 1} \sum_{j=0}^{N_y - 1} \int_{K_{i,j}} (f(u(\boldsymbol{x},t)) - f(u_{i,j}(t))) \, d\boldsymbol{x} \\ &+ \frac{1}{|\Omega|} \sum_{i=0}^{N_x - 1} \sum_{j=0}^{N_y - 1} \int_{K_{i,j}} (f(u(\boldsymbol{x}_{i,j},t)) - f(\bar{u}_{i,j}(t))) \, d\boldsymbol{x} = \mathcal{M}(f(\bar{u}_{i,j}(t))) + O(h^2), \end{split}$$

where the fact that $x_{i,j}$ is the center of the cell $K_{i,j}$ and (21) are used. Therefore,

$$\bar{f}(u_{i,j}(t)) = \bar{f}(\bar{u}(\boldsymbol{x}_{i,j},t)) + O(h^2).$$
 (23)

Following Proposition 2.2 and [29], both the numerical solution $\bar{U}_h(t)$ and the exact solution u(x,t) are bounded in the maximum norm by β . Therefore, the nonlinearity can be controlled easily [29], and by Duhamel's Principle, we can obtain the estimate (20) in view of (21), (22) and (23). The details are omitted here for brevity.

We then apply the ETD schemes for temporal integration of the stabilized space-discrete system (19). For this space-discrete case, we have the semigroup $\mathcal{S}_{\mathcal{L}_{\kappa,h}}(t) = e^{\mathcal{L}_{\kappa,h}t}$, which is a matrix exponential. Denoting \bar{U}_h^n as the numerical approximation of $\bar{U}_h(t_n)$, we compute \bar{U}_h^{n+1} as follows:

• First-order ETD scheme (denoted as $\bar{U}_h^{n+1} = \text{sETD1-MAC}(\bar{U}_h^n, \tau)$)

$$\bar{U}_h^{n+1} = e^{\mathcal{L}_{\kappa,h}\tau} \bar{U}_h^n + \int_0^\tau e^{\mathcal{L}_{\kappa,h}(\tau-s)} \bar{f}_{\kappa}(\bar{U}_h^n) ds.$$

• Second-order ETDRK scheme (denoted as $\bar{U}_h^{n+1} = \text{sETDRK2-MAC}\left(\bar{U}_h^n, \tau\right)$)

$$\begin{cases} \tilde{\bar{U}}_h^{n+1} = \text{sETD1-MAC}\left(\bar{U}_h^n, \tau\right) \\ \bar{U}_h^{n+1} = e^{\mathcal{L}_{\kappa,h}\tau} \bar{U}_h^n + \int_0^\tau e^{\mathcal{L}_{\kappa,h}(\tau-s)} \left(\frac{\tau-s}{\tau} \bar{f}_\kappa(\bar{U}_h^n) + \frac{s}{\tau} \bar{f}_\kappa(\tilde{\bar{U}}_h^{n+1}) \right) ds. \end{cases}$$

Note that FFT-based fast algorithms can be easily used for the implementation of the above sETD1-MAC and sETDRK2-MAC stepping schemes, see [13, 29] for details.

3.3. High-dimension reconstruction

Reconstruction process is well-studied in ENO and WENO schemes [48] to obtain high-order fluxes. We will employ the 2D reconstruction based on the cell averages. Given the cell averages $\{\bar{u}_{i-2+m,j-2+n}\}_{m,n=0}^3$ on the cells $\{K_{i-2+m,j-2+n}\}_{m,n=0}^3$, our reconstruction process is to find the bi-quadratic polynomial $R_{i,j}(x,y)$, such that

$$\frac{1}{h^2} \int_{x_{i-2+m-\frac{1}{2}}}^{x_{i-2+m+\frac{1}{2}}} \int_{y_{j-2+n-\frac{1}{2}}}^{y_{j-2+n+\frac{1}{2}}} R_{i,j}(x,y) dx dy = \bar{u}_{i-2+m,j-2+n}, \quad 0 \le m, \ n \le 3.$$

In [48], the WENO interpolation and the WENO reconstruction were bridged by using the primitive function for the reconstruction polynomial. Following this way, we introduce the primitive function

$$r_{i,j}(x,y) = \int_{x_{i-\frac{5}{2}}}^{x} \int_{y_{j-\frac{5}{2}}}^{y} R_{i,j}(\eta,\xi) d\eta \, d\xi, \tag{24}$$

and it is clear that

$$r_{i,j}(x_{i-\frac{3}{2}+m}, y_{j-\frac{3}{2}+n}) = h^2 \sum_{p=0}^{m} \sum_{q=0}^{n} \bar{u}_{i-2+p, j-2+q}, \quad 0 \le m, n \le 3.$$
 (25)

We then consider the tensor-product Lagrangian interpolation (where the degree of each variable is at most 3) based on the values at the half-grid points from (25). The one-dimensional Lagrange interpolation functions on $\{x_{i-\frac{3}{2}+m}, 0 \leq m \leq 3\}$ and $\{y_{j-\frac{3}{2}+n}, 0 \leq m \leq 3\}$ are respectively given by

$$I_x^m(x) = \frac{\prod_{l \neq m} (x - x_{i - \frac{3}{2} + l})}{\prod_{l \neq m} (x_{i - \frac{3}{2} + m} - x_{i - \frac{3}{2} + l})}, \quad I_y^n(y) = \frac{\prod_{l \neq n} (y - y_{j - \frac{3}{2} + l})}{\prod_{l \neq n} (y_{j - \frac{3}{2} + n} - y_{j - \frac{3}{2} + l})}$$

for $0 \le m, n \le 3$. Therefore,

$$r_{i,j}(x,y) = h^2 \sum_{0 \le m,n \le 3} \sum_{p=0}^m \sum_{q=0}^n \bar{u}_{i-2+p,j-2+q} I_x^m(x) I_y^n(y).$$
 (26)

Since $R_{i,j}(x,y) = \frac{\partial^2 r_{i,j}(x,y)}{\partial x \partial y}$, we have

$$R_{i,j}(x,y) = h^2 \sum_{p=1}^{3} \sum_{q=1}^{3} \bar{u}_{i-2+p,j-2+q} \sum_{m=p}^{3} \sum_{n=q}^{3} \frac{dI_x^m(x)}{dx} \frac{dI_y^n(y)}{dy}$$

$$= h^2 \sum_{m=1}^{3} \sum_{n=1}^{3} \frac{dI_x^m(x)}{dx} \frac{dI_y^n(y)}{dy} \sum_{p=1}^{m} \sum_{q=1}^{n} \bar{u}_{i-2+p,j-2+q}.$$
(27)

For convenience, we list the derivatives $\frac{dI_x^m(x)}{dx}$ on the stencils associated with the center $K_{0,0}$ and h=1, while other cases can be treated via translation and scaling:

$$\frac{dI_x^1(x)}{dx} = \frac{1}{2} \left(3x^2 - x - \frac{9}{4} \right), \quad \frac{dI_x^2(x)}{dx} = -\frac{1}{2} \left(3x^2 + x - \frac{9}{4} \right), \quad \frac{dI_x^3(x)}{dx} = \frac{1}{6} \left(3x^2 + 3x - \frac{1}{4} \right).$$

By the interpolation properties, it is easy to prove the following result.

Lemma 3.4. Assume $u(x,y) \in C^3(\overline{\Omega})$ and let $R_{i,j}(x,y)$ be given in (27) on the cell $K_{i,j}$. For any $(x,y) \in K_{i,j}$, it holds $R_{i,j}(x,y) - u(x,y) = O(h^3)$.

3.4. Maximum-principle-satisfying finite volume method for the transport equation

Let us consider the transport equation:

$$\frac{\partial u}{\partial t} + \nabla \cdot (\mathbf{v}u) = 0, \tag{28}$$

with $u(0) = u_0$, where the impressible velocity field $\mathbf{v} = (v_1, v_2)$ and thus

$$\nabla \cdot (\mathbf{v}u) = (v_1 u)_x + (v_2 u)_y.$$

Note the above transport equation is to carry the order parameter u moving with the velocity \mathbf{v} , and thus under the periodic boundary condition it will not change the maximum and minimum values of u along the time, which is also called the maximum principle of the equation (28).

Introducing $\alpha_1 = \max |v_1(\boldsymbol{x},t)|$ and $\alpha_2 = \max |v_2(\boldsymbol{x},t)|$, where the maximums are taken over

 $(x,t) \in \Omega \times [0,T]$, the finite volume approximation of (28) in space is given by

$$\frac{\partial \bar{U}_{i,j}}{\partial t} = -\frac{1}{h^2} \int_{y_{j-\frac{1}{2}}}^{y_{j+\frac{1}{2}}} h_1[U_{i+\frac{1}{2},y}^-, U_{i+\frac{1}{2},y}^+] - h_1[U_{i-\frac{1}{2},y}^-, U_{i-\frac{1}{2},y}^+] dy
- \frac{1}{h^2} \int_{x_{i-\frac{1}{2}}}^{x_{i+\frac{1}{2}}} h_2[U_{x,j+\frac{1}{2}}^-, U_{x,j+\frac{1}{2}}^+] - h_2[U_{x,j-\frac{1}{2}}^-, U_{x,j-\frac{1}{2}}^+] dx,$$
(29)

with $\bar{U}_{i,j}(0) = (\bar{u}_0)_{i,j} := \frac{1}{h^2} \int_{K_{i,j}} u_0(\boldsymbol{x}) d\boldsymbol{x}$, where U^- and U^+ represent the left and right limits, respectively, and $h_1[\cdot,\cdot]$ and $h_2[\cdot,\cdot]$ are certain monotone fluxes. The Lax-Friedrichs fluxes are adopted in our work, i.e.,

$$h_1[u,w] = \frac{1}{2} (v_1 u + v_1 w - \alpha_1(w-u)), \quad h_2(u,w) = \frac{1}{2} (v_2 u + v_2 w - \alpha_2(w-u)).$$

To obtain the values at the half-grids, the reconstruction is needed based on the cell-averaged value \bar{U} . Assuming the reconstruction polynomial $R_{i,j}(x,y)$ is found through (27), the two integrals in (29) can be approximated by quadratures with sufficient accuracy due to Lemma 3.4. Here, we shall employ the Gaussian quadrature with 2 points, which is exact for single variable polynomials of degree 3. Denote $S_i^x = \{x_i^{\zeta}: \zeta = 1, 2\}$ as the Gaussian quadrature points on $[x_{i-\frac{1}{2}}, x_{i+\frac{1}{2}}]$, and $S_j^y = \{y_j^{\zeta}: \zeta = 1, 2\}$ the Gaussian quadrature points on $[y_{j-\frac{1}{2}}, y_{j+\frac{1}{2}}]$. For example, the Gaussian quadrature points on $[-\frac{1}{2}, \frac{1}{2}]$ are $\{-\frac{\sqrt{3}}{6}, \frac{\sqrt{3}}{6}\}$ with the corresponding weights $w_1 = \frac{1}{2}$, and $w_2 = \frac{1}{2}$. Meanwhile we also introduce the quadrature points $\hat{S}_i^x = \{x_i^{\mu}: \mu = 1, 2, 3\}$ as the Gauss-Lobatto quadrature points on $[x_{i-\frac{1}{2}}, x_{i+\frac{1}{2}}]$, and $\hat{S}_j^y = \{y_j^{\mu}: \mu = 1, 2, 3\}$ the Gauss-Lobatto quadrature points on $[y_{j-\frac{1}{2}}, y_{j+\frac{1}{2}}]$. For instance, the Gauss-Lobatto quadrature points on $[-\frac{1}{2}, \frac{1}{2}]$ are $\{-\frac{1}{2}, 0, \frac{1}{2}\}$ with the corresponding weights $w_{\mu} = \{\frac{1}{6}, \frac{2}{3}, \frac{1}{6}\}$. On the generic cell $K_{i,j}$, we denote $x_{i+\frac{1}{2},\zeta}$ as the point $(x_{i+\frac{1}{2}}, y_j^{\zeta})$ and $x_{\zeta,j+\frac{1}{2}}$ as the point $(x_i^{\zeta}, y_{j+\frac{1}{2}})$. The same rule applies for other grid points with the subscripts ζ and μ . The forward Euler scheme for time integration of (29) for (28) then reads: given \bar{U}^n , compute

$$\bar{U}_{i,j}^{n+1} = \bar{U}_{i,j}^n - \tau \mathcal{F}_{i,j}(\bar{U}^n), \tag{30}$$

where

$$\mathcal{F}_{i,j}(\bar{U}^n) = \sum_{\zeta=1}^{2} \left(h_1[U_{i+\frac{1}{2},\zeta}^{n-}, U_{i+\frac{1}{2},\zeta}^{n+}] - h_1[U_{i-\frac{1}{2},\zeta}^{n-}, U_{i-\frac{1}{2},\zeta}^{n+}] \right) + h_2[U_{\zeta,j+\frac{1}{2}}^{n-}, U_{\zeta,j+\frac{1}{2}}^{n+}] - h_2[U_{\zeta,j-\frac{1}{2}}^{n-}, U_{\zeta,j-\frac{1}{2}}^{n+}] \frac{w_{\zeta}}{h}.$$

The CFL condition of the above forward Euler scheme is that

$$(\alpha_1 + \alpha_2) \frac{\tau}{h} \le \frac{1}{6},\tag{31}$$

However, $\bar{U}_{i,j}^{n+1}$ obtained from (30) with the values on the half-grid quadrature points evaluated by $R_{i,j}^n(x,y)$ generally does not satisfy the maximum principle possessed by the transport equation (28), where the superscript n indicates the dependency on the values at $t=t_n$. X. Zhang and C.-W. Shu [61] designed an efficient limiter approach to bound the maximum and minimum values on the quadrature points, and we will adopt their strategy in this work.

Define the special quadrature point set $S_{i,j} = \left(S_i^x \otimes S_j^y\right) \cup \left(S_i^x \otimes \hat{S}_j^y\right) \cup \left(\hat{S}_i^x \otimes S_j^y\right) \cup \left(\hat{S}_i^x \otimes S_j^y\right$

S1. Use the two-dimensional cell averages to obtain the reconstruction polynomial $R_{i,j}^n(x,y)$:

$$\{\bar{U}_{i,j}^n\} \xrightarrow{\text{reconstruction}} R_{i,j}^n(x,y).$$

S2. Calculate the values of $R_{i,j}^n(x,y)$ on the quadrature point set $S_{i,j}$, and find the limiter θ on each cell such that

$$\theta = \min \left\{ \left| \frac{M_{\beta} - U_{i,\zeta}^n}{M_{i,j}^n - U_{i,\zeta}^n} \right|, \left| \frac{m_{\beta} - U_{i,\zeta}^n}{m_{i,j}^n - U_{i,\zeta}^n} \right|, 1 \right\},$$
(32)

where $M_{i,j}^n = \max_{(x,y) \in S_{i,j}} R_{i,j}^n(x,y)$ and $m_{i,j}^n = \min_{(x,y) \in S_{i,j}} R_{i,j}^n(x,y)$. Here M_{β} and m_{β} are the maximum and minimum values of the exact solution u (which will be specified later in our complete numerical schemes for the MACAC equation).

S3. Evaluate the half-grid point values via the following polynomial

$$\tilde{R}_{i,j}^{n}(x,y) = \theta(R_{i,j}^{n}(x,y) - \bar{U}_{i,j}^{n}) + \bar{U}_{i,j}^{n}.$$
(33)

which is then plugged into (30) to update $\bar{U}_{i,j}^{n+1}$.

Remark 3.5. As shown in [61, 62, 31], the transport velocity field \mathbf{v} plays an important role on preserving the maximum bound, and the divergence-free property should be maintained locally on each cell. The required CFL condition (31) is usually more strict than that allowed by the ETD schemes used for the MCAC equation in Section 3.2. As a consequence, we better conduct the substepping to evolve the transport equation from t_n to t_{n+1} as needed.

The above 3 steps (S1,S2,S3) perform one step of the forward Euler scheme, and we shall refer such one Euler step as

$$\bar{U}_h^{n+1} = \text{MP-FEuler-Transport} (\bar{U}_h^n, t_n, \tau, M_\beta, m_\beta).$$

As shown in [61], "MP-FEuler-Transport" can maintain the accuracy of the scheme for smooth solutions. More generally, if the substepping is used from t_n to t_{n+1} , we denote such process as

$$\bar{U}_h^{n+1} = \text{MP-FEuler-Transport-Substep}(\bar{U}_h^n, t_n, \tau, M, M_\beta, m_\beta)$$

where M denotes the number of substeps and each substep is a one forward Euler stepping with the small time step size $\frac{\tau}{M}$. To achieve second-order temporal accuracy, we use the second-order explicit strong stability preserving Runge-Kutta (SSPRK2) scheme which consists of two forward Euler steps at each time step:

$$\begin{cases} \hat{\bar{U}}_{i,j}^{n+1} = \bar{U}_{i,j}^{n} - \tau \mathcal{F}_{i,j}(\bar{U}^{n}), \\ \hat{\bar{U}}_{i,j}^{n+1} = \frac{1}{2}\bar{U}_{i,j}^{n} + \frac{1}{2}(\hat{\bar{U}}_{i,j}^{n+1} - \tau \mathcal{F}_{i,j}(\hat{\bar{U}}^{n+1})). \end{cases}$$
(34)

We refer the corresponding SSPRK2 substepping from t_n to t_{n+1} for (28) as

$$\bar{U}_h^{n+1} = \text{MP-SSPRK2-Transport-Substep} (\bar{U}_h^n, t_n, \tau, M, M_\beta, m_\beta),$$

which contains M substeps of the SSPRK2 stepping with the small time step size $\frac{\tau}{M}$.

Lemma 3.6. Suppose that $\mathbf{v} \in C^1((0,T); [C^3(\Omega)]^2)$ and $u \in C^2((0,T); C^4(\Omega))$ is the exact solution to the transport equation (28). Under the CFL condition (31), there exists a constant C > 0 independent of τ and h, such that

$$||u(\cdot, t_{n+1}) - \bar{U}_h^*||_{\infty, h} \le ||u(\cdot, t_n) - \bar{U}_h^n||_{\infty, h} + C(\tau^2 + \tau h^2), \quad 0 \le n \le N - 1.$$
(35)

where \bar{U}_h^n is any approximation of $u(\cdot,t_n)$ with $||u(\cdot,t_n)-\bar{U}_h^n||_{\infty,h}=O(h^2)$ and

$$\bar{U}_h^* = \text{MP-FEuler-Transport-Substep} (\bar{U}_h^n, t_n, \tau, M, M_\beta, m_\beta).$$

Proof. Let $\bar{u}_{i,j}(t)$ be the cell average of u(t) over the cell $K_{i,j} \in \Omega_h$. Since $R_{i,j}(x,y)$ is the reconstruction polynomial defined by (27), for any $(x,y) \in K_{i,j}$, Taylor expansion gives

$$u(\boldsymbol{x},t) = u(\boldsymbol{x}_{i,j},t) + \nabla u(\boldsymbol{x}_{i,j}) \cdot (\boldsymbol{x} - \boldsymbol{x}_{i,j}) + \frac{1}{2}(\boldsymbol{x} - \boldsymbol{x}_{i,j})^2 :: (\nabla \nabla u(\boldsymbol{x}_{i,j},t)) + O(h^3), \quad (36)$$

and $\bar{u}_{i,j}(t) - u(\boldsymbol{x}_{i,j},t) = O(h^2)$. Taking the integral of (28) over $K_{i,j}$, we have

$$\begin{split} \frac{d\bar{u}(\boldsymbol{x}_{i,j},t)}{dt} &= -\frac{1}{h^2} \int_{y_{j-\frac{1}{2}}}^{y_{j+\frac{1}{2}}} h_1[u(x_{i+\frac{1}{2}},y),u(x_{i+\frac{1}{2}},y)] - h_1[u(x_{i-\frac{1}{2}},y),u(x_{i-\frac{1}{2}},y)]dy \\ &- \frac{1}{h^2} \int_{x_{i-\frac{1}{2}}}^{x_{i+\frac{1}{2}}} h_2[u(x,y_{j+\frac{1}{2}}),u(x,y_{j+\frac{1}{2}})] - h_2[u(x,y_{j-\frac{1}{2}}),u(x,y_{j-\frac{1}{2}})]dx. \end{split} \tag{37}$$

It is also easy to see that

$$\frac{d\bar{u}(\boldsymbol{x}_{i,j},t)}{dt}\Big|_{t=t_n} = \frac{du(\boldsymbol{x}_{i,j},t)}{dt}\Big|_{t=t_n} + O(h^2)$$

$$= \frac{u(\boldsymbol{x}_{i,j},t_{n+\frac{1}{M}}) - u(\boldsymbol{x}_{i,j},t_n)}{\tau/M} - \frac{\tau}{2M}\frac{d^2u(\boldsymbol{x}_{i,j},t_n)}{dt^2} + O\left(\frac{\tau^2}{M^2} + h^2\right).$$
(38)

By the interpolation properties, $u(\mathbf{x}) = \tilde{R}_{i,j}(x,y) + O(h^3)$ for any $\mathbf{x} \in K_{i,j}$ ($\tilde{R}_{i,j}$ is the modified reconstruction polynomial according to the numerical limiter on $K_{i,j}$ in (33)), (37) and (38) then lead to

$$\begin{split} u(\boldsymbol{x}_{i,j},t_{n+\frac{1}{M}}) &= u(\boldsymbol{x}_{i,j},t_n) - \frac{\tau}{Mh} \sum_{\zeta=1}^{2} \left(h_1[\tilde{R}_{i+\frac{1}{2},\zeta}^{u,n},\tilde{R}_{i+\frac{1}{2},\zeta}^{u,n}] - h_1[\tilde{R}_{i-\frac{1}{2},\zeta}^{u,n},\tilde{R}_{i-\frac{1}{2},\zeta}^{u,n}] \right) w_{\zeta} \\ &- \frac{\tau}{Mh} \sum_{\zeta=1}^{2} \left(h_2[\tilde{R}_{\zeta,j+\frac{1}{2}}^{u,n},\tilde{R}_{\zeta,j+\frac{1}{2}}^{u,n}] - h_2[\tilde{R}_{\zeta,j-\frac{1}{2}}^{u,n},\tilde{R}_{\zeta,j-\frac{1}{2}}^{u,n}] \right) w_{\zeta} + \frac{\tau^2}{2M^2} \frac{d^2u(\boldsymbol{x}_{i,j},t_n)}{dt^2} \\ &+ C\left(\frac{\tau h^2}{M} + \frac{\tau^3}{M^3} \right), \end{split}$$

where C is a generic positive constant independent of h and τ , and $\tilde{R}^{u,n}_{i+\frac{1}{2},\zeta} = \tilde{R}^{u,n}_{i,j}(x_{i+\frac{1}{2}},y_{\zeta})$ with

the superscript u indicates that the reconstruction is decided from the values of u.

Let $e^n = \left(e^n_{i,j}\right)_{N_x \times N_y}$ with $e^n_{i,j} = u^n(\boldsymbol{x}_{i,j}) - \bar{U}^n_{i,j}$. For the transport equation (28), h_1 and h_2 are linear in both $u(\boldsymbol{x}_{i,j},t_n)$ and $\bar{U}^n_{i,j}$ once the coordinates are specified and the parameter θ in the modified reconstruction on cell $K_{i,j}$ is fixed (the one used in the reconstruction for updating $\bar{U}^{n+1}_{i,j}$). Subtracting (30) from the above equation, we can obtain the error equation as follows:

$$e_{i,j}^{n+1/M} = e_{i,j}^{n} - \frac{\tau}{Mh} \sum_{\zeta=1}^{2} \left(h_{1} [\tilde{R}_{i+\frac{1}{2},\zeta}^{e,n}, \tilde{R}_{i+\frac{1}{2},\zeta}^{e,n}] - h_{1} [\tilde{R}_{i-\frac{1}{2},\zeta}^{e,n}, \tilde{R}_{i-\frac{1}{2},\zeta}^{e,n}] \right) w_{\zeta}$$

$$- \frac{\tau}{Mh} \sum_{\zeta=1}^{2} \left(h_{2} [\tilde{R}_{\zeta,j+\frac{1}{2}}^{e,n}, \tilde{R}_{\zeta,j+\frac{1}{2}}^{e,n}] - h_{2} [\tilde{R}_{\zeta,j-\frac{1}{2}}^{e,n}, \tilde{R}_{\zeta,j-\frac{1}{2}}^{e,n}] \right) w_{\zeta} + C \left(\frac{\tau h^{2}}{M} + \frac{\tau^{2}}{M^{2}} \right).$$

Next we replace the polynomial $\tilde{R}^{e,n}(x,y)$ by the modified reconstruction polynomial $\tilde{R}^{e,n}(x,y)$ with the limiter (32) determined by $e_{i,j}^n$ with $\max\{e_{i,j}^n\}$ and $\min\{e_{i,j}^n\}$ replacing M_β and m_β , respectively. By Lemma 3.4, extra errors of $O(h^3)$ would be introduced and we have

$$e_{i,j}^{n+1/M} = e_{i,j}^{n} - \frac{\tau}{Mh} \sum_{\zeta=1}^{2} \left(h_{1} [\tilde{\tilde{R}}_{i+\frac{1}{2},\zeta}^{e,n}, \tilde{\tilde{R}}_{i+\frac{1}{2},\zeta}^{e,n}] - h_{1} [\tilde{\tilde{R}}_{i-\frac{1}{2},\zeta}^{e,n}, \tilde{\tilde{R}}_{i-\frac{1}{2},\zeta}^{e,n}] \right) w_{\zeta}$$

$$- \frac{\tau}{Mh} \sum_{\zeta=1}^{2} \left(h_{2} [\tilde{\tilde{R}}_{\zeta,j+\frac{1}{2}}^{e,n}, \tilde{\tilde{R}}_{\zeta,j+\frac{1}{2}}^{e,n}] - h_{2} [\tilde{\tilde{R}}_{\zeta,j-\frac{1}{2}}^{e,n}, \tilde{\tilde{R}}_{\zeta,j-\frac{1}{2}}^{e,n}] \right) w_{\zeta} + C \left(\frac{\tau h^{2}}{M} + \frac{\tau^{2}}{M^{2}} \right).$$

By the CFL condition, the above reconstruction using $\tilde{R}^{e,n}(x,y)$ is maximum bound preserving, which immediately implies

$$||e^{n+1/M}||_{\infty,h} \le ||e^n||_{\infty,h} + C\left(\frac{\tau h^2}{M} + \frac{\tau^2}{M^2}\right).$$
 (39)

Applying the telescoping on (39) from t_n to t_{n+1} , we can obtain (35) which completes the proof. \square

Lemma 3.7. Suppose that $\mathbf{v} \in C^2((0,T); [C^3(\Omega)]^2)$ and $u \in C^3((0,T); C^4(\Omega))$ is the exact solution to the transport equation (28). Under the CFL condition (31), there exists a constant C > 0 independent of τ and h, such that

$$||u(\cdot, t_{n+1}) - \bar{U}_h^{**}||_{\infty, h} \le ||u(\cdot, t_n) - \bar{U}_h^n||_{\infty, h} + C(\tau^3 + \tau h^2), \quad 0 \le n \le N - 1.$$

$$(40)$$

where \bar{U}_h^n is any approximation of $u(\cdot,t_n)$ with $||u(\cdot,t_n) - \bar{U}_h^n||_{\infty,h} = O(h^2)$ and

$$\bar{U}_h^{**} = \text{MP-SSPRK2-Transport-Substep} (\bar{U}_h^n, t_n, \tau, M, M_\beta, m_\beta).$$

Proof. The SSPRK2 stepping with the step size $\frac{\tau}{M}$ can be expressed as

$$\begin{cases} \tilde{\bar{U}}_{i,j}^{n+1/M} = \bar{U}_{i,j}^n - \frac{\tau}{M} \mathcal{F}(\bar{U}_{i,j}^n), \\ \bar{U}_{i,j}^{n+1/M} = \frac{1}{2} \bar{U}_{i,j}^n + \frac{1}{2} \left(\tilde{\bar{U}}_{i,j}^{n+1/M} - \frac{\tau}{M} \mathcal{F}(\tilde{\bar{U}}_{i,j}^{n+1/M}) \right). \end{cases}$$

Correspondingly, the exact solution $u(\mathbf{x}_{i,j}, t_n + \tau/M)$ satisfies

$$\begin{cases} \tilde{u}_{i,j}^{n+1/M} = u(\boldsymbol{x}_{i,j}, t_n) - \frac{\tau}{M} \mathcal{F}(u(\boldsymbol{x}_{i,j}, t_n)) = u(\boldsymbol{x}_{i,j}, t_{n+1/M}) + O\left(\frac{\tau}{M} h^2\right), \\ u(\boldsymbol{x}_{i,j}, t_{n+1/M}) = \frac{1}{2} u(\boldsymbol{x}_{i,j}, t_n) + \frac{1}{2} \tilde{u}_{i,j}^{n+1/M} - \frac{\tau}{2M} \left(\mathcal{F}(\tilde{u}_{i,j}^{n+1/M}) + O(h^2)\right) + O\left(\frac{\tau^3}{M^3}\right). \end{cases}$$

Under the CFL condition, the above equation gives

$$\|u(\boldsymbol{x}_{i,j},t_{n+1/M}) - \bar{U}_{i,j}^{n+1/M}\|_{\infty,h}$$

$$\leq \frac{1}{2}\|u(\boldsymbol{x}_{i,j},t_n) - \bar{U}_{i,j}^n\|_{\infty,h} + \frac{1}{2}\|\tilde{u}_{i,j}^{n+1/M} - \tilde{\bar{U}}_{i,j}^{n+1/M}\|_{\infty,h} + O\left(\frac{\tau^3}{M^3} + \frac{\tau h^2}{M}\right)$$

$$\leq \|u(\boldsymbol{x}_{i,j},t_n) - \bar{U}_{i,j}^n\|_{\infty,h} + O\left(\frac{\tau^3}{M^3} + \frac{\tau h^2}{M}\right).$$

Let $e^n = \left(e_{i,j}^n\right)_{N_x \times N_y}$ with $e_{i,j}^n = u(\boldsymbol{x}_{i,j},t_n) - \bar{U}_{i,j}^n$ be the error function. The error growth can be controlled as

$$||e^{n+1/M}||_{\infty,h} \le ||e^n||_{\infty,h} + O\left(\frac{\tau^3}{M^3} + \frac{\tau h^2}{M}\right).$$
 (41)

Applying the telescoping on (41) from t_n to t_{n+1} , we can obtain (40) which completes the proof.

Remark 3.8. For the phase-field equation coupling with the incompressible Navier-Stokes or other equations, the velocities at the fractional steps are not available. As a remedy, one could borrow the idea from local time-stepping methods [19, 18] and interpolate the velocities for those values.

4. Fully-discrete structure-preserving schemes and error analysis

Now, we are ready to present the operator splitting based fully-discrete structure-preserving schemes for the MCAC equation (12) (or (5)) and corresponding error analysis.

Given
$$\bar{U}_h^0 = \bar{U}_h(0)$$
 with $\{\bar{U}_{i,j}(0) = (\bar{u}_0)_{i,j}\}$, for $n = 0, 1, \dots, N-1$, compute \bar{U}_h^{n+1} by:

• First-order (in time) scheme (MBP-FEuler-sETD1):

$$\begin{cases}
\bar{U}_{h}^{*,n+1} = \text{sETD1-MAC}(\bar{U}_{h}^{n}, \tau), \\
\bar{U}_{h}^{n+1} = \text{MP-FEuler-Transport-Substep}(\bar{U}_{h}^{*,n+1}, t_{n}, \tau, M, M_{\beta}, m_{\beta}) \\
\text{with } M_{\beta} = \max\{\bar{U}_{h}^{*,n+1}\}, \ m_{\beta} = \min\{\bar{U}_{h}^{*,n+1}\}.
\end{cases} (42)$$

• Second-order (in time) scheme (MBP-SSPRK2-sETDRK2):

$$\begin{cases} \bar{U}_{h}^{*,n+1/2} = \text{sETDRK2-MAC} (\bar{U}_{h}^{n}, \frac{\tau}{2}), \\ \bar{U}_{h}^{**,n+1} = \text{MP-SSPRK2-Transport-Substep} (\bar{U}_{h}^{*,n+1/2}, t_{n}, \tau, M, M_{\beta}, m_{\beta}) \\ \text{with } M_{\beta} = \max\{\bar{U}_{h}^{*,n+1/2}\}, \ m_{\beta} = \min\{\bar{U}_{h}^{*,n+1/2}\}, \\ \bar{U}_{h}^{n+1} = \text{sETDRK2-MAC} (\bar{U}_{h}^{**,n+1}, \frac{\tau}{2}). \end{cases}$$
(43)

Remark 4.1. In the above MBP-FEuler-sETD1 and MBP-SSPRK2-sETDRK2 schemes, at the second stage of each time step, we set M_{β} and m_{β} as the maximum and minimum values of the ETD solution of the MAC equation from the first stage, instead of β and $-\beta$, due to the important fact that the transport equation does not change the maximum and minimum values of the solution imposed by its initial values under the periodic boundary condition.

4.1. Structure preservation

Now we show the proposed MBP-FEuler-sETD1 and MBP-SSPRK2-sETDRK2 schemes preserve the discrete maximum bound principle and conserve the total mass.

Lemma 4.2. (Discrete MBP) Suppose that Assumption 2.1 and the requirement (13) are satisfied. The schemes (42) (MBP-FEuler-sETD1) and (43) (MBP-SSPRK2-sETDRK2) preserve the discrete MBP under the CFL condition (31), i.e., if $(\alpha_1 + \alpha_2) \frac{\tau}{Mh} \leq \frac{1}{6}$ and $\|\bar{U}_h^0\|_{\infty,h} \leq \beta$, then $\|\bar{U}_h^0\|_{\infty,h} \leq \beta$ for any $n \geq 0$.

Proof. It suffices to prove that each component of the schemes (42) and (43) preserves the maximum bound. First of all, it is shown in [29] that the stabilized ETD method preserves the discrete MBP unconditionally for the MAC equation. Secondly, the discrete MBP of the MP-FEuler-Transport scheme is proved under the CFL condition (31) in [61]. Moreover, the SSPRK2 stepping is just a convex combination of two forward Euler steps (indeed it is a TVD scheme). Therefore, the MBP-preservation of the MP-SSPRK2-Transport-Substep follows.

Lemma 4.3. (Mass conservation) Suppose that Assumption 2.1 and the requirement (13) are satisfied. The schemes (42) (MBP-FEuler-sETD1) and (43) (MBP-SSPRK2-sETDRK2) conserve the mass under the CFL condition, i.e., if $(\alpha_1 + \alpha_2)\frac{\tau}{h} \leq \frac{1}{6}$, then

$$\mathcal{M}(\bar{U}_h^N) = \mathcal{M}(\bar{U}_h^{N-1}) = \dots = \mathcal{M}(\bar{U}_h^0). \tag{44}$$

Proof. We only need to show that the mass is conserved by each component of the schemes (42) and (43). First, according to [29, Lemma 4.1 and 4.2], we have for MBP-FEuler-sETD1,

$$h^{2} \sum_{i=0}^{N_{x}-1} \sum_{j=0}^{N_{y}-1} \bar{U}_{h}^{*,n+1} = h^{2} \sum_{i=0}^{N_{x}-1} \sum_{j=0}^{N_{y}-1} \bar{U}_{h}^{n},$$

and for MBP-SSPRK2-sETDRK2,

$$\begin{cases} h^2 \sum_{i=0}^{N_x - 1} \sum_{j=0}^{N_y - 1} \bar{U}_h^{*,n + \frac{1}{2}} = h^2 \sum_{i=0}^{N_x - 1} \sum_{j=0}^{N_y - 1} \bar{U}_h^n, \\ h^2 \sum_{i=0}^{N_x - 1} \sum_{j=0}^{N_y - 1} \bar{U}_h^{n+1} = h^2 \sum_{i=0}^{N_x - 1} \sum_{j=0}^{N_y - 1} \bar{U}_h^{**,n+1}. \end{cases}$$

Now we are only left with proving the mass-conservation of the MP-FEuler-Transport with M=1.

Summing (30) over $i = 0, ..., N_x - 1$ and $j = 0, ..., N_y - 1$ yields

$$\begin{split} \sum_{i=0}^{N_x-1} \sum_{j=0}^{N_y-1} \bar{U}_{i,j}^{n+1} &= \sum_{i=0}^{N_x-1} \sum_{j=0}^{N_y-1} \bar{U}_{i,j}^{n} - \tau \sum_{\zeta=1}^{2} \sum_{j=0}^{N_y-1} \sum_{i=0}^{N_x-1} \left(h_1[U_{i+\frac{1}{2},\zeta}^{n-1},U_{i+\frac{1}{2},\zeta}^{n+1}] - h_1[U_{i-\frac{1}{2},\zeta}^{n-1},U_{i-\frac{1}{2},\zeta}^{n+1}] \right) w_\zeta \\ &- \tau \sum_{\zeta=1}^{2} \sum_{i=0}^{N_x-1} \sum_{j=0}^{N_y-1} \left(h_2[U_{\zeta,j+\frac{1}{2}}^{n-1},U_{\zeta,j+\frac{1}{2}}^{n+1}] - h_2[U_{\zeta,j-\frac{1}{2}}^{n-1},U_{\zeta,j-\frac{1}{2}}^{n+1}] \right) w_\zeta, \end{split}$$

where the periodic boundary condition implies

$$\sum_{i=0}^{N_x-1} \left(h_1[U^{n-}_{i+\frac{1}{2},\zeta},U^{n+}_{i+\frac{1}{2},\zeta}] - h_1[U^{n-}_{i-\frac{1}{2},\zeta},U^{n+}_{i-\frac{1}{2},\zeta}] \right) = h_1[U^{n-}_{N_x-\frac{1}{2},\zeta},U^{n+}_{N_x-\frac{1}{2},\zeta}] - h_1[U^{n-}_{-\frac{1}{2},\zeta},U^{n+}_{-\frac{1}{2},\zeta}] = 0.$$

The other terms vanish similarly, thus MP-FEuler-Transport conserves the mass, i.e.,

$$\sum_{i=0}^{N_x-1} \sum_{j=0}^{N_y-1} \bar{U}_{i,j}^{n+1} = \sum_{i=0}^{N_x-1} \sum_{j=0}^{N_y-1} \bar{U}_{i,j}^{n},$$

which completes the proof.

4.2. Error estimates

Now we present the error estimates for the schemes (42) (MBP-FEuler-sETD1) and (43) (MBP-SSPRK2-sETDRK2).

Theorem 4.4. (Error estimate of MBP-FEuler-sETD1) Suppose that Assumption 2.1 and the requirement (13) are satisfied, the velocity field $\mathbf{v} \in C^1((0,T);[C^3(\Omega)]^2)$, the exact solution u to the MCAC equation (5) belongs to $C^2((0,T);C^4(\Omega))$, and the initial data $||u_0(\cdot)||_{\infty} \leq \beta$. Let $\{\bar{U}_h^n\}_{n\geq 0}$ be the numerical solution generated by the MBP-FEuler-sETD1 scheme (42). Then for any sufficiently small τ and h satisfying the CFL condition (31), it holds

$$||u(\cdot,t_n) - \bar{U}_h^n||_{\infty,h} \le C\left(\tau + h^2\right), \quad 0 \le n \le N, \tag{45}$$

where the constant C > 0 is independent of τ and h.

Proof. Let $u^n(\mathbf{x})$ ($\mathbf{x} \in \Omega$) be the numerical solution obtained by the first-order operator splitting scheme (14). Lemma 3.1 indicates that, in order to obtain (45) it suffices to show that there exists a constant C > 0 independent of h and τ , such that

$$||u^n - \bar{U}_h^n||_{\infty,h} \le C(\tau + h^2), \quad 0 \le n \le N.$$
 (46)

When n=0, it is is trivial by the choice of the initialization \bar{U}_h^0 . For the simplicity, we denote u_I^n as the restrictions of u^n on the grid points Ω_h (the same notations will apply to other functions defined on Ω). We note that the MBP property ensures $u^n(\boldsymbol{x})$ and \bar{U}_h^n are point-wisely bounded by β in absolute value, and the nonlinear function f (and \bar{f}_{κ}) can be treated as a Lipschitz function.

From t_n to t_{n+1} for $n \geq 0$, based on the assumptions of the theorem and the properties of the semilinear parabolic equations and transport equations, $u^*(\boldsymbol{x}, s)$ and $u^{**}(\boldsymbol{x}, s)$ ($\boldsymbol{x} \in \Omega, s \in [0, \tau]$)

in (14) are sufficiently smooth. On the domain Ω_h , $u_I^*(0) = u_I^n$, and by the finite difference discretization, we have for $s \in [0, \tau]$,

$$\frac{\partial u_I^*(\boldsymbol{x},s)}{\partial s} = \mathcal{L}_{\kappa,h} u_I^*(\boldsymbol{x},s) + \bar{f}_{\kappa}(u_I^n(\boldsymbol{x})) + O(\tau + h^2), \quad \boldsymbol{x} \in \Omega_h.$$
(47)

The Duhamel's principle implies,

$$u_I^*(\tau) = e^{\mathcal{L}_{\kappa,h}\tau} u_I^n + \int_0^{\tau} e^{\mathcal{L}_{\kappa,h}(\tau-s)} \bar{f}_{\kappa}(u_I^n) ds + O(\tau h^2 + \tau^2).$$

Define the error function $\mathcal{E}^n(\boldsymbol{x}) = u_I^n(\boldsymbol{x}) - \bar{U}_h^n(\boldsymbol{x})$ for $\boldsymbol{x} \in \Omega_h$ and $n \geq 0$. Subtracting the first equation in the scheme (42) from the above equation, we obtain

$$u_{I}^{*}(\tau) - \bar{U}^{*,n+1} = e^{\mathcal{L}_{\kappa,h}\tau} \mathcal{E}^{n} + \int_{0}^{\tau} e^{\mathcal{L}_{\kappa,h}(\tau-s)} (\bar{f}_{\kappa}(u_{I}^{n}) - \bar{f}_{\kappa}(\bar{U}_{h}^{n})) ds + O(\tau h^{2} + \tau^{2}).$$

Recalling the MBP property, by the discrete version of Lemma 2.3 [29, 13], Lemmas 2.4 and 3.3, we can get

$$||u^*(\tau) - \bar{U}^{*,n+1}||_{\infty,h} \le e^{-\kappa\tau} ||\mathcal{E}^n||_{\infty,h} + 3\kappa ||\mathcal{E}^n||_{\infty,h} \int_0^\tau e^{-\kappa(\tau-s)} ds + O(\tau^2 + \tau h^2). \tag{48}$$

Next, thanks to Lemma 3.6, the estimate on the second part of the scheme (42) can be given as

$$\|\mathcal{E}^{n+1}\|_{\infty,h} = \|u^{**}(\tau) - \bar{U}_h^{n+1}\|_{\infty,h} \le \|u^*(\tau) - \bar{U}^{*,n+1}\|_{\infty,h} + C(\tau^2 + \tau h^2). \tag{49}$$

Combining (48) with (49), noticing $1 - s \le e^{-s} \le 1 + s$ (s > 0), we get

$$\|\mathcal{E}^{n+1}\|_{\infty,h} \le e^{-\kappa\tau} \|\mathcal{E}^{n}\|_{\infty,h} + 3\kappa \|\mathcal{E}^{n}\|_{\infty,h} \frac{1 - e^{-\kappa\tau}}{\kappa} + C(\tau^{2} + \tau h^{2})$$

$$< (1 + 2\kappa\tau) \|\mathcal{E}^{n}\|_{\infty,h} + C(\tau^{2} + \tau h^{2}), \quad 0 < n < N - 1.$$
(50)

Thus, the discrete Gronwall inequality with (50) and $\|\mathcal{E}^0\|_{\infty,h} = O(h^2)$ gives (46), which completes the proof.

Theorem 4.5. (Error estimate of MBP-SSPRK2-sETDRK2) Suppose that Assumption 2.1 and the requirement (13) are satisfied, the velocity field $\mathbf{v} \in C^2((0,T); [C^3(\Omega)]^2)$ and $u \in C^3((0,T); C^4(\Omega))$ is the exact solution to the MCAC equation (5), and the initial data $\|u_0(\cdot)\|_{\infty} \leq \beta$. Let $\{\bar{U}_h^n\}_{n\geq 0}$ be the numerical solution generated by the MBP-SSPRK2-sETDRK2 scheme (43). Then for any sufficiently small τ and h satisfying the CFL condition (31), it holds

$$||u(\cdot, t_n) - \bar{U}_h^n||_{\infty, h} \le C(\tau^2 + h^2), \quad 0 \le n \le N,$$
 (51)

where the constant C > 0 is independent of τ and h.

Proof. Let $u^n(x)$ ($x \in \Omega$) be the numerical solution obtained by the second-order Strang operator splitting scheme (16). Lemma 3.2 ensures that, in order to obtain (51) it suffices to show that there

exists a constant C > 0 independent of h and τ , such that

$$||u^n(\cdot) - \bar{U}_h^n||_h \le C(\tau^2 + h^2), \quad 0 \le n \le N.$$
 (52)

Following the notations and arguments in the proof of Theorem 4.4, from t_n to $t_n + 1$ for $n \ge 0$, based on the first step of the scheme (16), we can get

$$u_I^*\left(\frac{\tau}{2}\right) = e^{\mathcal{L}_{\kappa,h}\frac{\tau}{2}}u_I^n + \int_0^{\frac{\tau}{2}} e^{\mathcal{L}_{\kappa,h}\left(\frac{\tau}{2} - s\right)} \left(\frac{\tau - 2s}{\tau}\bar{f}_{\kappa}(u_I^n) + \frac{2s}{\tau}\bar{f}_{\kappa}\left(u_I^*\left(\frac{\tau}{2}\right)\right)\right) ds + O(\tau^3 + \tau h^2),$$

Recalling the error function $\mathcal{E}^n(\boldsymbol{x}) = u_I^n(\boldsymbol{x}) - \bar{U}_h^n(\boldsymbol{x})$ and subtracting the first equation in the scheme (43) from the above equation, we have

$$\begin{split} u_I^*\left(\frac{\tau}{2}\right) - \bar{U}_h^{*,n+\frac{1}{2}} &= e^{\mathcal{L}_{\kappa,h}\frac{\tau}{2}}\mathcal{E}^n + \int_0^{\frac{\tau}{2}} e^{\mathcal{L}_{\kappa,h}(\frac{\tau}{2}-s)} \left(\frac{\tau-2s}{\tau} \left(\bar{f}_\kappa(u_I^n) - \bar{f}_\kappa(\bar{U}_h^n)\right)\right) ds \\ &+ \int_0^{\frac{\tau}{2}} e^{\mathcal{L}_{\kappa,h}(\frac{\tau}{2}-s)} \left(\frac{2s}{\tau} \left(\bar{f}_\kappa \left(u_I^*\left(\frac{\tau}{2}\right)\right) - \bar{f}_\kappa(\tilde{U}_h^{*,n+\frac{1}{2}})\right)\right) ds + O(\tau^3 + \tau h^2), \end{split}$$

where $\tilde{\bar{U}}_h^{*,n+\frac{1}{2}} = \text{sETD1-MAC}(\bar{U}_h^n, \frac{\tau}{2})$. From (48), we have

$$\|u_I^*\left(\frac{\tau}{2}\right) - \tilde{U}_h^{*,n+\frac{1}{2}}\|_{\infty,h} \le (3 - 2e^{-\kappa\frac{\tau}{2}})\|\mathcal{E}^n\|_{\infty,h} + C(\tau^2 + \tau h^2).$$

Using the MBP property, we can proceed to get

$$\|u_{I}^{*}\left(\frac{\tau}{2}\right) - \bar{U}_{h}^{*,n+\frac{1}{2}}\|_{\infty,h} \leq e^{-\kappa\frac{\tau}{2}} \|\mathcal{E}^{n}\|_{\infty,h} + 3\kappa \|U^{*}\left(\cdot,\frac{\tau}{2}\right) - \tilde{\bar{U}}_{h}^{*,n+\frac{1}{2}}\|_{\infty,h} \int_{0}^{\frac{\tau}{2}} \frac{2s}{\tau} e^{-\kappa(\frac{\tau}{2}-s)} ds + 3\kappa \|\mathcal{E}^{n}\|_{\infty,h} \int_{0}^{\frac{\tau}{2}} \frac{\tau - 2s}{\tau} e^{-\kappa(\frac{\tau}{2}-s)} ds + C(\tau^{3} + \tau h^{2})$$

$$\leq (1 + 9\kappa\tau) \|\mathcal{E}^{n}\|_{\infty,h} + C(\tau^{3} + \tau h^{2}).$$

$$(53)$$

By Lemma 3.7, under the CFL condition, we have the following estimate on the second equation in the scheme (43):

$$\|u_I^{**}(\tau) - \bar{U}_h^{**,n+1}\|_{\infty,h} \le \|u_I^*\left(\frac{\tau}{2}\right) - \bar{U}_h^{*,n+\frac{1}{2}}\|_{\infty,h} + C(\tau h^2 + \tau^3). \tag{54}$$

Next, by the similar arguments for deriving (53), we obtain

$$\|\mathcal{E}^{n+1}\|_{\infty,h} \le (1+9\kappa\tau)\|u_I^{**}(\tau) - \bar{U}_h^{**,n+1}\|_{\infty,h} + C(\tau h^2 + \tau^3).$$
(55)

Combing (53)-(55), for some constant $C_{\kappa} > 0$ depending on κ , we reach

$$\|\mathcal{E}^{n+1}\|_{\infty,h} \le (1 + C_{\kappa}\tau)\|\mathcal{E}^n\|_{\infty,h} + C(\tau h^2 + \tau^3), \quad 0 \le n \le N - 1.$$
 (56)

Thus, the discrete Gronwall inequality with (56) and $\|\mathcal{E}^0\|_{\infty,h} = O(h^2)$ gives us (52), which completes the proof.

5. Numerical experiments

In this section, we present various numerical examples to verify the theoretical results and demonstrate the performance of the proposed two schemes, MBP-FEuler-sETD1 (42) and MBP-SSPRK2-sETDRK2 (43), for solving the MCAC equation (5). The computational domain is set to be $\Omega = [0, 1]^d$.

5.1. Convergence tests

We consider the MCAC equation (5) in two dimensions (d=2) with the initial condition

$$u_0(x,y) = \cos(2\pi x)\cos(2\pi y),$$

and the thickness parameter $\epsilon = 0.1$. In addition, the nonlinear reaction f = -F' is given by the double-well potential case, i.e., $f(u) = u - u^3$, and thus the bounding constant $\beta = \frac{2\sqrt{3}}{3}$. The stabilizing coefficient is chosen as $\kappa = 3$ to satisfy the requirement (13). The terminal time is set to be T = 0.5. We choose the velocity field

$$\mathbf{v} = e^{-t} [\sin(2\pi y), \sin(2\pi x)]^T.$$

The solution obtained by MBP-SSPRK2-sETDRK2 with h=1/1024 and $\tau=1/2048$ is adopted as the benchmark solution for computing the numerical errors at the terminal time. We first set M=1, which means that no substepping is used in the transport equation solver. With τ decreasing by a factor of 2, h decreasing by a factor of roughly $\sqrt{2}$ for MBP-FEuler-sETD1 and 2 for MBP-SSPRK2-sETDRK2. The numerical results on the discrete L^{∞} and L^2 errors along the time-space grid refinement and corresponding convergence rates are reported in Table 1. The first-order convergence is clearly observed for MBP-FEuler-sETD1, and for MBP-SSPRK2-sETDRK2, the convergent rates initially are higher than two but gradually decreases to be close to two. Next, we test the effect of substepping M=10. We use MBP-SSPRK2-sETDRK2 with h=1/1024 and $\tau=1/1024$ to generate the benchmark solution. The numerical results on the discrete L^{∞} and L^2 errors along the time-space grid refinement and corresponding convergence rates are reported in Table 2. We again observe the similar convergence behavior as that of the case of M=1.

Table 1: Numerical results on the discrete L^{∞} and L^2 errors and corresponding convergence rates for the MBP-FEuler-sETD1 and MBP-SSPRK2-sETDRK2 schemes with M=1.

au	MBP-FEuler-sETD1					MBP-SSPRK2-sETDRK2				
	h	L^{∞} Error	Rate	L^2 Error	Rate	h	L^{∞} Error	Rate	L^2 Error	Rate
-1/32	1/16	1.1274e-01	-	5.6793e-02	-	1/16	6.7898e-02	-	2.6305 e-02	_
1/64	1/23	4.8982e-02	1.20	2.5412e-02	1.16	1/32	1.2884 e-02	2.40	4.6348e-03	2.50
1/128	1/32	2.4268e-02	1.01	1.2344e-02	1.04	1/64	1.6587e-03	2.96	6.8019 e-04	2.77
1/256	1/45	1.2895 e-02	0.91	6.1584 e-03	1.00	1/128	3.0517e-04	2.44	1.2386e-04	2.46
1/512	1/64	6.8748e-03	0.91	3.1424 e-03	0.97	1/256	7.0718e-05	2.11	2.8486e-05	2.12

5.2. MBP tests

In this subsection, we numerically investigate the discrete MBP of the proposed schemes in longtime phase separation processes governed by the MCAC equation (5) with the thickness parameter

Table 2: Numerical results on the discrete L^{∞} and L^2 errors and corresponding convergence rates for the MBP-FEuler-sETD1 and MBP-SSPRK2-sETDRK2 schemes with M=10.

au	MBP-FEuler-sETD1					MBP-SSPRK2-sETDRK2				
	h	L^{∞} Error	Rate	L^2 Error	Rate	h	L^{∞} Error	Rate	L^2 Error	Rate
$\frac{1}{16}$	1/16	4.4959e-01	-	2.1578e-01	-	1/16	8.9967e-02	-	3.1431e-02	_
1/32	1/23	1.5397e-01	1.55	7.4041e-02	1.54	1/32	1.9435e-02	2.21	7.4245 e - 03	2.08
1/64	1/32	6.4828 e-02	1.25	3.0636e-02	1.27	1/64	3.4128e-03	2.51	1.6692e-03	2.15
1/128	1/45	3.0456e-02	1.09	1.3926e-02	1.14	1/128	8.1959e-04	2.06	3.9305 e-04	2.09
1/256	1/64	1.4907e-02	1.03	6.7183e-03	1.05	1/256	1.9468e-04	2.07	9.1946 e - 05	2.10

 $\epsilon = 0.01$. For simplicity, we only test MBP-SSPRK2-sETDRK2 (43) since the basic components of MBP-FEuler-sETD1 are similar. We start the simulations at time t = 0 with the initial configuration given by

$$u_0(x,y) = 0.9\sin(20\pi x)\sin(20\pi y),$$

and the cell-averaged quantities are computed accordingly. The convection velocity field is again set to be

$$\mathbf{v} = e^{-t} [\sin(2\pi y), \sin(2\pi x)]^T,$$

which eventually approaches to zeros when the time t becomes very large. The time step size, the number of substeps (for the transport equation solver), and the spatial grid size are chosen as $\tau = 0.01$, M = 10, and h = 1/256, respectively.

We first test the case of double-well potential function (8) with the bounding constant $\beta = \frac{2\sqrt{3}}{3}$ and the stabilizing constant $\kappa = 3$. Figure 1 presents the configurations of the numerical solutions at the times t = 0.5, 30, 70, 100, 150, and 200 respectively, which shows a steady-state is gradually reached along the time evolution. The dynamics of the supremum norm, mass and energy (defined in (1)) are plotted in Figure 2. It is observed that the discrete MBP is well preserved where the red solid line is $y = \frac{2\sqrt{3}}{3}$ which gives the theoretical maximum bound. Furthermore, we find the supremum norm of the numerical solution in fact quickly approaches the red dashed line y = 1 which is the maximum bound of the classic AC equation in this case. In addition, it is easy to see that the mass is numerically conserved perfectly and the energy (defined by (1)) decays monotonically along the time (although theoretically the energy dissipation law is not guaranteed anymore for the MCAC equation).

Next we test the case of Flory-Huggins potential function (9) with the parameters $\theta = 0.8$ and $\theta_c = 1.6$. The bounding constant is now $\beta \approx 0.9868$ for this case and the stabilizing coefficient is taken as $\kappa = 28.87$ to satisfy the requirement (13). Figure 3 presents the configurations of the numerical solution at t = 0.5, 30, 70, 100, 150, and 200 respectively. The corresponding dynamics of the supremum norm, mass and energy are plotted in Figure 4. It is shown that the discrete MBP is well preserved, the mass is perfectly conserved, and the energy decays monotonically along the time. In this case, the red solid red is y = 0.9868 which gives the theoretical maximum bound, but we find that the supremum norm of the numerical solution again quickly approaches the red dash line y = 0.9575 which is the maximum bound of the classic AC equation. By comparing the coarsening phenomena in Figures 1 and 3, we observe that both cases of potential functions produce very similar steady states at the end although they follows some different intermediate dynamics

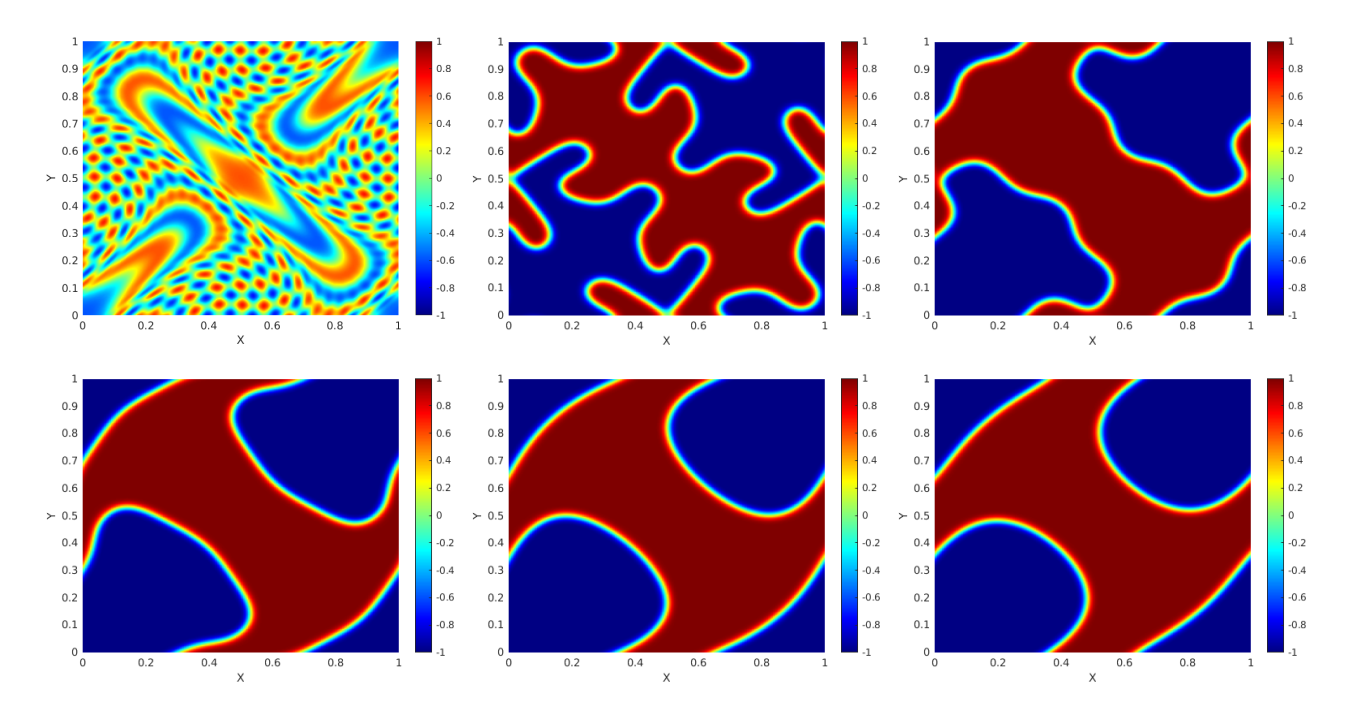


Figure 1: Numerical solutions at the times t = 0.5, 30, 70, 100, 150, and 200 respectively (from left to right) for the MCAC equation (5) with the double well potential (8) in two dimensions.

along the time evolution.

5.3. 3D simulations

In this subsection, some 3D simulations are reported for the MCAC equation with $\epsilon = 0.01$. The initial configuration is the quasi-uniform state obtained by setting $u_0 = 1.8(\text{rand}(\cdot) - 0.5)$, where $\text{rand}(\cdot)$ is the Matlab function which generates pseudorandom values from the standard uniform distribution on the open interval (0,1). The velocity field is chosen as

$$\mathbf{v} = [y - 0.5, 0.5 - x, 0]^T,$$

which is time-independent and rotates around the center (0.5, 0.5) in the xy-plane at each vertical level. We use MBP-SSPRK2-sETDRK2 (43) to simulate the case of double-well potential function (8), thus the stabilizing coefficient $\kappa=3$ is used. The other used parameters are $\tau=0.01$, M=10, and h=1/128. Figure 5 shows the iso-surfaces formed by the zero level set (i.e. u=0) of the numerical solution and the snapshots of the two cross-sections z=0.5 and x=0.5 at the times t=0,1,5, and 20 respectively. The ordering and grain coarsening process are clearly observed along the time evolution, together with the rotating behavior in the xy-plane due to the specially imposed velocity field. The corresponding evolutions of the supremum norm, mass increments (comparing to the initial mass) and energy are shown in Figure 6. It is again easy to see that the energy decays monotonically, and the discrete MBP and mass equation are perfectly preserved.

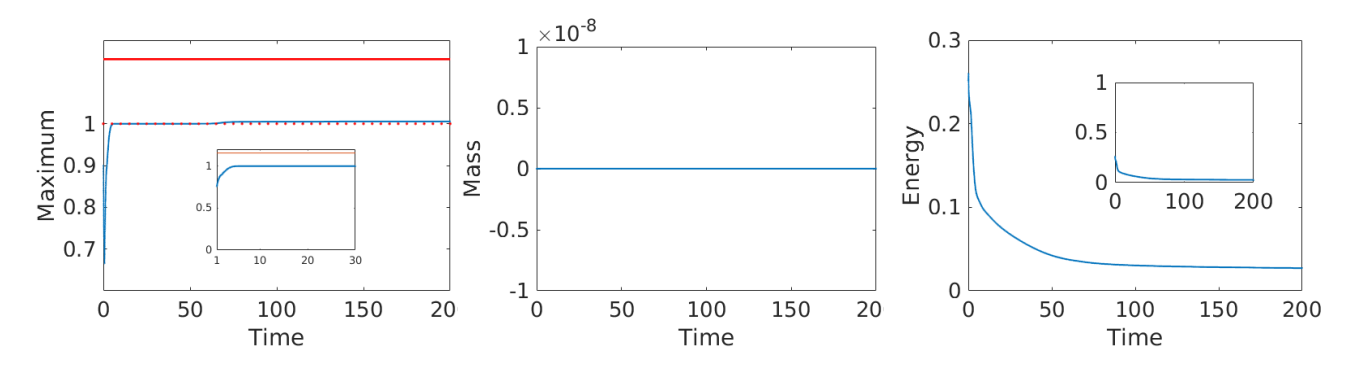


Figure 2: Evolution of the supremum norm (left), mass (middle), and energy (right) of the numerical solution for the MCAC equation (5) with the double well potential (8) in two dimensions.

6. Conclusion

In this paper we have developed two structure-preserving numerical schemes, MBP-FEulersETD1 and MBP-SSPRK2-sETDRK2, for solving the MCAC equation based on the operator splitting approach. Each time stepping of the MCAC equation is split into two (first-order splitting in time) or three (second-order splitting in time) stages, each of them consisting of either a MAC equation or a transport equation. For the MAC part, the finite volume approximation is applied for spatial discretization and then the stabilized exponential time differencing schemes are used for time integration. Note that FFT-based fast algorithm can be used to efficiently calculate the matrix exponential acting on the vectors in the implementation of the MAC solver. For the transport part, the explicit SSPRK method for time integration is combined with a limiter-based maximumprinciple-satisfying finite volume discretization in space, in which a substepping procedure is also adopted to deal with the CFL condition in order to match large time step sizes allowed by the MAC solver. In addition to preservation of the discrete MBP and conservation of the mass, we also show that, while MBP-FEuler-sETD1 is first-order accurate in time and MBP-SSPRK2-sETDRK2 is second-order accurate in time, both schemes are second-order accurate in space. Various numerical examples are also presented to verify the theoretical results and demonstrate the performance of the proposed schemes. As an important application, the MCAC equation is one of the essential components for phase field modeling of the multiphase fluid system coupled with a flow field described by Stokes or Navier-Stokes equations, thus how to extend the proposed schemes to solution of such more complex models is subject to our future research.

Acknowledgement

L. Ju's work was partially supported by U.S. National Science Foundation grant DMS-2109633. J. Li's work was partially supported by China Postdoctoral Science Foundation grant 2021M700476. Y. Cai's work was partially supported by Natural Science Foundation of China grants 12171041 and 11771036.

References

[1] S. M. Allen and J. W. Cahn. A microscopic theory for antiphase boundary motion and its application to antiphase domain coarsening. *Acta Metallurgica*, 27(6):1085–1095, 1979.

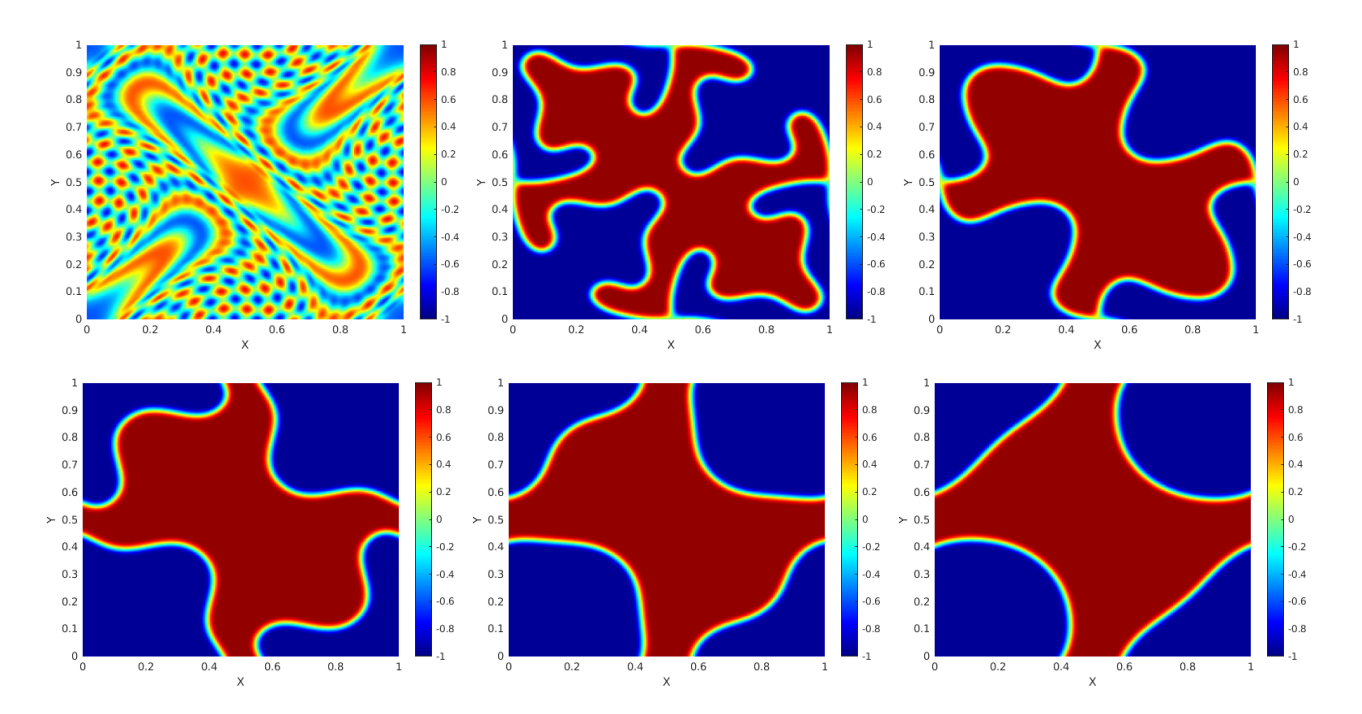


Figure 3: Numerical solutions at the times t = 0.5, 30, 70, 100, 150, and 200 respectively (from left to right) for the MCAC equation (5) with the Flory-Huggins potential (9) in two dimensions.

- [2] D. M. Anderson, G. B. McFadden, and A. A. Wheeler. Diffuse-interface methods in fluid mechanics. *Annual Review of Fluid Mechanics*, 30(1):139–165, 1998.
- [3] G. Beylkin, J. M. Keiser, and L. Vozovoi. A new class of time discretization schemes for the solution of nonlinear PDEs. *Journal of Computational Physics*, 147(2):362–387, 1998.
- [4] J. W. Cahn and J. E. Hilliard. Free energy of a nonuniform system. i. interfacial free energy. *The Journal of Chemical Physics*, 28(2):258–267, 1958.
- [5] Y. Cai, L. Ju, R. Lan, and J. Li. Stabilized exponential time differencing schemes for the convective Allen-Cahn equation. *Communications in Mathematical Sciences*, to appear.
- [6] W. Chen, W. Feng, Y. Liu, C. Wang, and S. M. Wise. A second order energy stable scheme for the Cahn-Hilliard-Hele-Shaw equations. *Discrete and Continuous Dynamical Systems B*, 24(1):149–182, 2019.
- [7] W. Chen, W. Li, Z. Luo, C. Wang, and X. Wang. A stabilized second order exponential time differencing multistep method for thin film growth model without slope selection. *ESAIM: Mathematical Modelling and Numerical Analysis*, 54(3):727–750, 2020.
- [8] W. Chen, Y. Liu, C. Wang, and S. Wise. Convergence analysis of a fully discrete finite difference scheme for the Cahn-Hilliard-Hele-Shaw equation. *Mathematics of Computation*, 85(301):2231–2257, 2016.
- [9] K. Cheng, Z. Qiao, and C. Wang. A third order exponential time differencing numerical scheme

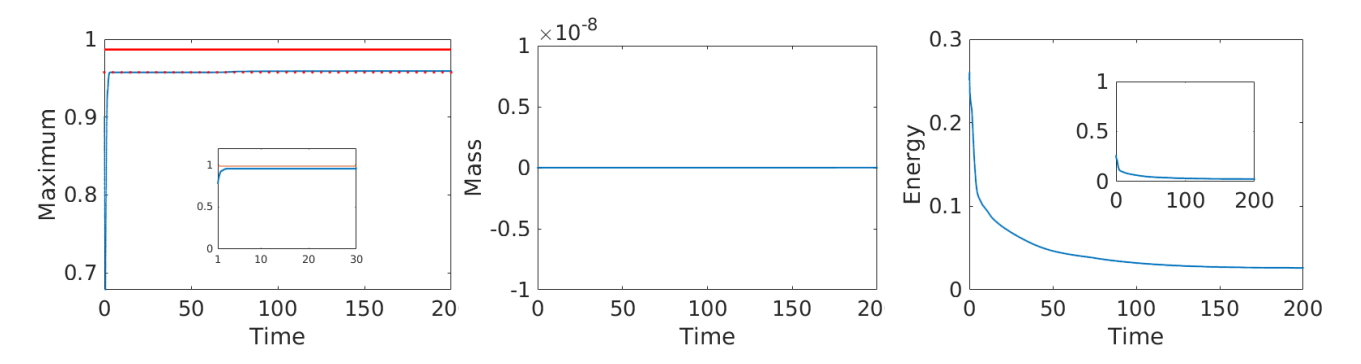


Figure 4: Evolution of the supremum norm (left), mass (middle), and energy (right) for the MCAC equation (5) with the Flory-Huggins potential (9) in two dimensions.

for no-slope-selection epitaxial thin film model with energy stability. *Journal of Scientific Computing*, 81(1):154–185, 2019.

- [10] S. M. Cox and P. C. Matthews. Exponential time differencing for stiff systems. *Journal of Computational Physics*, 176(2):430–455, 2002.
- [11] A. E. Diegel, C. Wang, X. Wang, and S. M. Wise. Convergence analysis and error estimates for a second order accurate finite element method for the Cahn–Hilliard–Navier–Stokes system. *Numerische Mathematik*, 137(3):495–534, 2017.
- [12] Q. Du, L. Ju, X. Li, and Z. Qiao. Maximum principle preserving exponential time differencing schemes for the nonlocal Allen-Cahn equation. SIAM Journal on Numerical Analysis, 57(2):875–898, 2019.
- [13] Q. Du, L. Ju, X. Li, and Z. Qiao. Maximum bound principles for a class of semilinear parabolic equations and exponential time differencing schemes. *SIAM Review*, 63(2):317–359, 2021.
- [14] K.-J. Engel and R. Nagel. One-parameter semigroups for linear evolution equations. In *Semi-group forum*, volume 63, pages 278–280. Springer, 2001.
- [15] L. Evans. *Partial Differential Equations*. Graduate studies in mathematics. American Mathematical Society, 2010.
- [16] S. Gaudreault, G. Rainwater, and M. Tokman. Kiops: A fast adaptive krylov subspace solver for exponential integrators. *Journal of Computational Physics*, 372:236–255, 2018.
- [17] M. E. Gurtin, D. Polignone, and J. Vinals. Two-phase binary fluids and immiscible fluids described by an order parameter. *Mathematical Models and Methods in Applied Sciences*, 6(06):815–831, 1996.
- [18] T.-T.-P. Hoang, L. Ju, W. Leng, and Z. Wang. High order explicit local time stepping methods for hyperbolic conservation laws. *Mathematics of Computation*, 89(324):1807–1842, 2020.
- [19] T.-T.-P. Hoang, W. Leng, L. Ju, Z. Wang, and K. Pieper. Conservative explicit local timestepping schemes for the shallow water equations. *Journal of Computational Physics*, 382:152– 176, 2019.

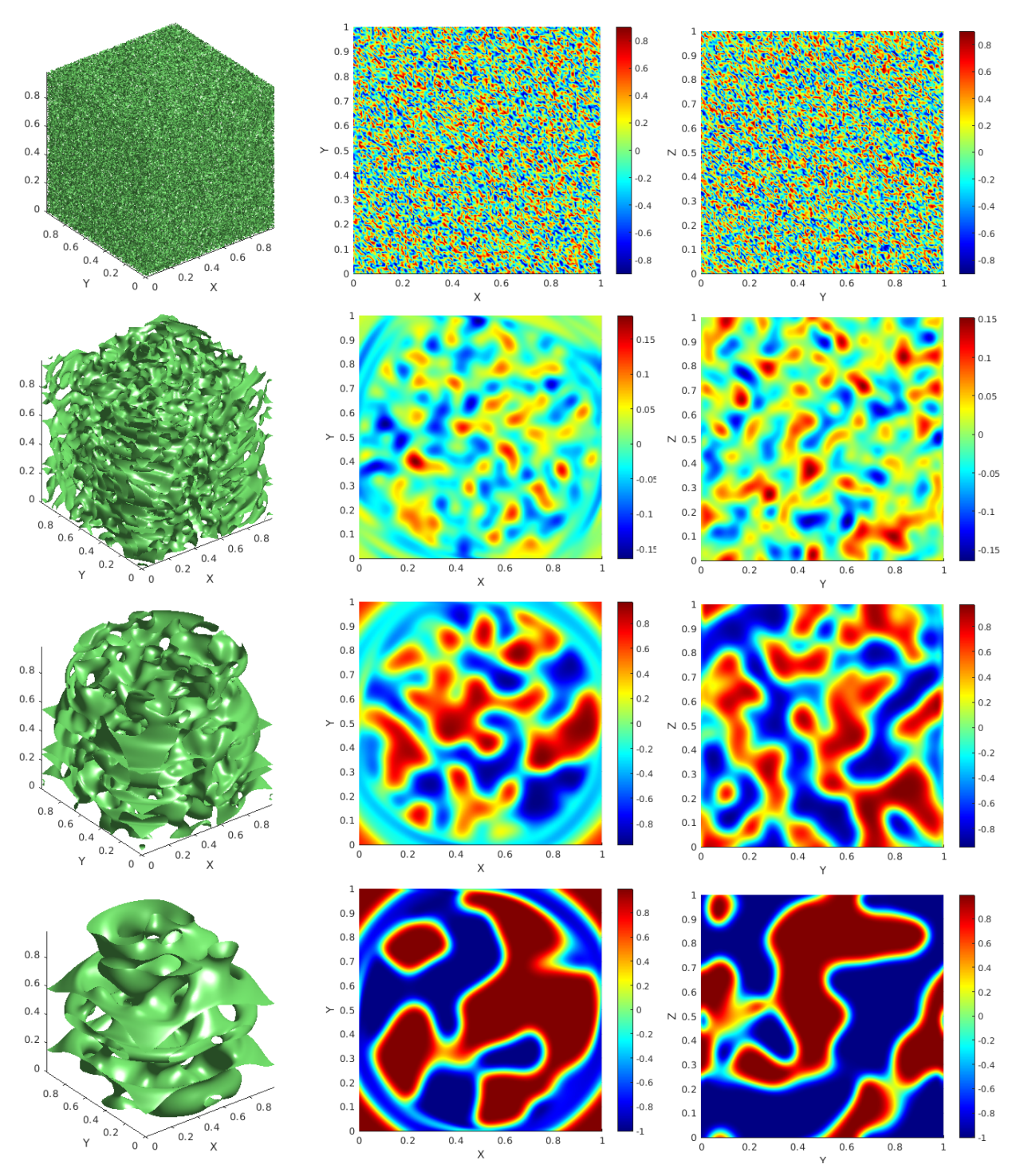


Figure 5: The iso-surfaces of u=0 (left), the snapshots of the cross-sections, z=0.5 (middle) and x=0.5 at the times $t=0,\,1,\,5,\,$ and 20 for the MCAC equation (5) with the double well potential in three dimensions.

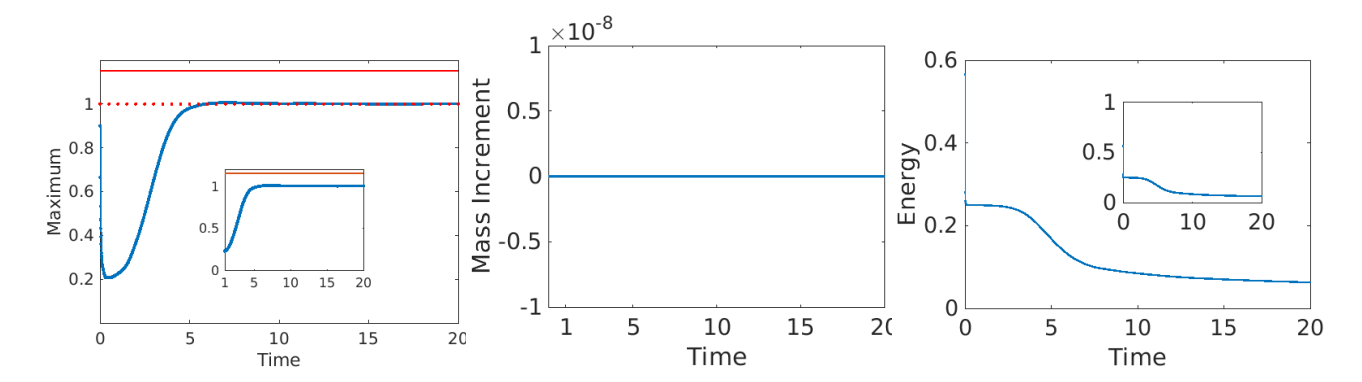


Figure 6: Evolution of the supremum norm (left), mass increment (middle) and energy (right) of the numerical solution for the MCAC equation (5) with the double well potential in three dimensions.

- [20] M. Hochbruck and A. Ostermann. Explicit exponential Runge-Kutta methods for semilinear parabolic problems. SIAM Journal on Numerical Analysis, 43(3):1069–1090, 2005.
- [21] W. Hundsdorfer and J. G. Verwer. Numerical solution of time-dependent advection-diffusion-reaction equations, volume 33. Springer Science & Business Media, 2007.
- [22] L. Isherwood, Z. J. Grant, and S. Gottlieb. Strong stability preserving integrating factor Runge-Kutta methods. SIAM Journal on Numerical Analysis, 56(6):3276–3307, 2018.
- [23] K. Jiang, L. Ju, J. Li, and X. Li. Unconditionally stable exponential time differencing schemes for the mass-conserving Allen-Cahn equation with nonlocal and local effects. *Numerical Methods for Partial Differential Equations*, 38:1636–1657, 2022.
- [24] L. Ju, X. Li, Z. Qiao, and J. Yang. Maximum bound principle preserving integrating factor Runge-Kutta methods for semilinear parabolic equations. *Journal of Computational Physics*, 439:110405, 2021.
- [25] L. Ju, J. Zhang, and Q. Du. Fast and accurate algorithms for simulating coarsening dynamics of Cahn-Hilliard equations. Computational Materials Science, 108:272–282, 2015.
- [26] L. Ju, J. Zhang, L. Zhu, and Q. Du. Fast explicit integration factor methods for semilinear parabolic equations. *Journal of Scientific Computing*, 62(2):431–455, 2015.
- [27] D. Lee. The numerical solutions for the energy-dissipative and mass-conservative Allen–Cahn equation. Computers & Mathematics with Applications, 80(1):263–284, 2020.
- [28] B. Li, J. Yang, and Z. Zhou. Arbitrarily high-order exponential cut-off methods for preserving maximum principle of parabolic equations. SIAM Journal on Scientific Computing, 42(6):A3957–A3978, 2020.
- [29] J. Li, L. Ju, Y. Cai, and X. Feng. Unconditionally maximum bound principle preserving linear schemes for the conservative Allen-Cahn equation with nonlocal constraint. *Journal of Scientific Computing*, 87(3):1–32, 2021.

- [30] J. Li, X. Li, L. Ju, and X. Feng. Stabilized integrating factor Runge-Kutta method and unconditional preservation of maximum bound principle. SIAM Journal on Scientific Computing, 43(3):A1780-A1802, 2021.
- [31] M. Li, Y. Cheng, J. Shen, and X. Zhang. A bound-preserving high order scheme for variable density incompressible Navier-Stokes equations. *Journal of Computational Physics*, 425:109906, 2021.
- [32] X. Li, L. Ju, and X. Meng. Convergence analysis of exponential time differencing schemes for the Cahn-Hilliard equation. *Communications in Computational Physics*, 26(5):1510–1529, 2019.
- [33] X. Li, Z. Qiao, and H. Zhang. Convergence of a fast explicit operator splitting method for the epitaxial growth model with slope selection. SIAM Journal on Numerical Analysis, 55(1):265–285, 2017.
- [34] H.-L. Liao, T. Tang, and T. Zhou. On energy stable, maximum-principle preserving, second-order BDF scheme with variable steps for the Allen–Cahn equation. *SIAM Journal on Numerical Analysis*, 58(4):2294–2314, 2020.
- [35] H.-L. Liao, T. Tang, and T. Zhou. A second-order and nonuniform time-stepping maximumprinciple preserving scheme for time-fractional Allen-Cahn equations. *Journal of Computa*tional Physics, 414:109473, 2020.
- [36] C. Liu, C. Wang, and Y. Wang. A structure-preserving, operator splitting scheme for reaction-diffusion equations with detailed balance. *Journal of Computational Physics*, 436:110253, 2021.
- [37] C. Liu, C. Wang, Y. Wang, and S. M. Wise. Convergence analysis of the variational operator splitting scheme for a reaction-diffusion system with detailed balance. *SIAM Journal on Numerical Analysis*, 60(2):781–803, 2022.
- [38] X.-D. Liu and S. Osher. Nonoscillatory high order accurate self-similar maximum principle satisfying shock capturing schemes i. *SIAM Journal on Numerical Analysis*, 33(2):760–779, 1996.
- [39] X.-D. Liu, S. Osher, and T. Chan. Weighted essentially non-oscillatory schemes. *Journal of Computational Physics*, 115(1):200–212, 1994.
- [40] Y. Liu, W. Chen, C. Wang, and S. M. Wise. Error analysis of a mixed finite element method for a Cahn–Hilliard–Hele–Shaw system. *Numerische Mathematik*, 135(3):679–709, 2017.
- [41] C. Moler and C. Van Loan. Nineteen dubious ways to compute the exponential of a matrix, twenty-five years later. SIAM Review, 45(1):3–49, 2003.
- [42] G. Peng, Z. Gao, and X. Feng. A stabilized extremum-preserving scheme for nonlinear parabolic equation on polygonal meshes. *International Journal for Numerical Methods in Fluids*, 90(7):340–356, 2019.
- [43] M. H. Protter and H. F. Weinberger. *Maximum principles in differential equations*. Springer Science & Business Media, 2012.

- [44] J. Rubinstein and P. Sternberg. Nonlocal reaction-diffusion equations and nucleation. *IMA Journal of Applied Mathematics*, 48(3):249–264, 1992.
- [45] J. Shen, T. Tang, and J. Yang. On the maximum principle preserving schemes for the generalized Allen-Cahn equation. *Communications in Mathematical Sciences*, 14(6):1517–1534, 2016.
- [46] J. Shen and X. Yang. A phase-field model and its numerical approximation for two-phase incompressible flows with different densities and viscosities. SIAM Journal on Scientific Computing, 32(3):1159–1179, 2010.
- [47] J. Shen and X. Zhang. Discrete maximum principle of a high order finite difference scheme for a generalized Allen-Cahn equation. *Communications in Mathematical Sciences*, 20(5):1409–1436, 2022.
- [48] C.-W. Shu. High order weighted essentially nonoscillatory schemes for convection dominated problems. SIAM Review, 51(1):82–126, 2009.
- [49] C.-W. Shu and S. Osher. Efficient implementation of essentially non-oscillatory shock-capturing schemes. *Journal of Computational Physics*, 77(2):439–471, 1988.
- [50] P. Strachota and M. Beneš. Error estimate of the finite volume scheme for the allen–cahn equation. *BIT Numerical Mathematics*, 58(2):489–507, 2018.
- [51] T. Tang and J. Yang. Implicit-explicit scheme for the Allen-Cahn equation preserves the maximum principle. *Journal of Computational Mathematics*, 34(5):471–481, 2016.
- [52] M. Taylor. Partial Differential Equations III: Nonlinear Equations, volume 117 of Applied Mathematical Sciences. Springer, 2011.
- [53] X. Xiao, Z. Dai, and X. Feng. A positivity preserving characteristic finite element method for solving the transport and convection-diffusion-reaction equations on general surfaces. Computer Physics Communications, 247:106941, 2020.
- [54] X. Xiao, R. He, and X. Feng. Unconditionally maximum principle preserving finite element schemes for the surface Allen-Cahn type equations. *Numerical Methods for Partial Differential Equations*, 36(2):418–438, 2020.
- [55] J. Yang, Z. Yuan, and Z. Zhou. Arbitrarily high-order maximum bound preserving schemes with cut-off postprocessing for Allen-Cahn equations. arXiv preprint arXiv:2102.13271, 2021.
- [56] X. Yang, J. Feng, C. Liu, and J. Shen. Numerical simulations of jet pinching-off and drop formation using an energetic variational phase-field method. *Journal of Computational Physics*, 218(1):417–428, 2006.
- [57] P. Yue, J. Feng, C. Liu, and J. Shen. Diffuse-interface simulations of drop coalescence and retraction in viscoelastic fluids. *Journal of Non-Newtonian Fluid Mechanics*, 129(3):163–176, 2005.

- [58] C. Zhang, H. Wang, J. Huang, C. Wang, and X. Yue. A second order operator splitting numerical scheme for the "good" Boussinesq equation. Applied Numerical Mathematics, 119:179–193, 2017.
- [59] G. Zhang, S. Zheng, and T. Xiong. A conservative semi-Lagrangian finite difference WENO scheme based on exponential integrator for one-dimensional scalar nonlinear hyperbolic equations. *Electronic Research Archive*, 29(1):1819–1839, 2021.
- [60] H. Zhang, J. Yan, X. Qian, X. Gu, and S. Song. On the preserving of the maximum principle and energy stability of high-order implicit-explicit Runge-Kutta schemes for the space-fractional Allen-Cahn equation. *Numerical Algorithms*, pages 1–28, 2021.
- [61] X. Zhang and C.-W. Shu. On maximum-principle-satisfying high order schemes for scalar conservation laws. *Journal of Computational Physics*, 229(9):3091–3120, 2010.
- [62] X. Zhang and C.-W. Shu. Maximum-principle-satisfying and positivity-preserving high-order schemes for conservation laws: survey and new developments. *Proceedings of the Royal Society A: Mathematical, Physical and Engineering Sciences*, 467(2134):2752–2776, 2011.